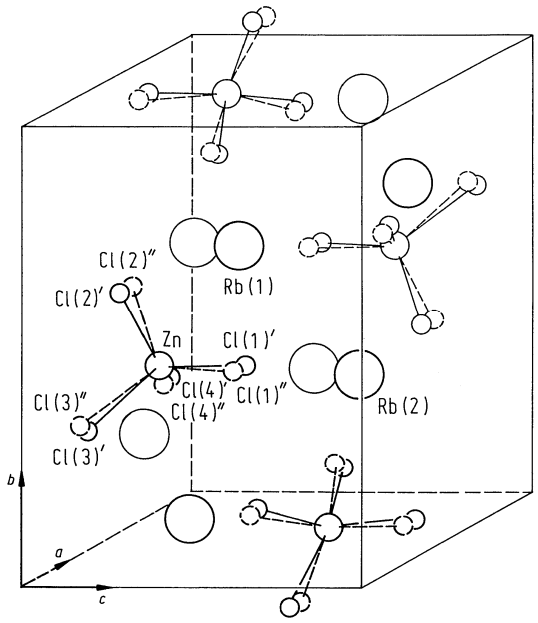

Fig. 39A-10-001. Rb_2ZnCl_4. Structure of phase I [83Ito]. T = 50 °C. View of the unit cell. Rb atoms and $ZnCl_4$ groups drawn with thick lines lie on x = 1/4 and thin lines on x = 3/4. Solid and broken lines of $ZnCl_4$ indicate two disordered arrangements, respectively.

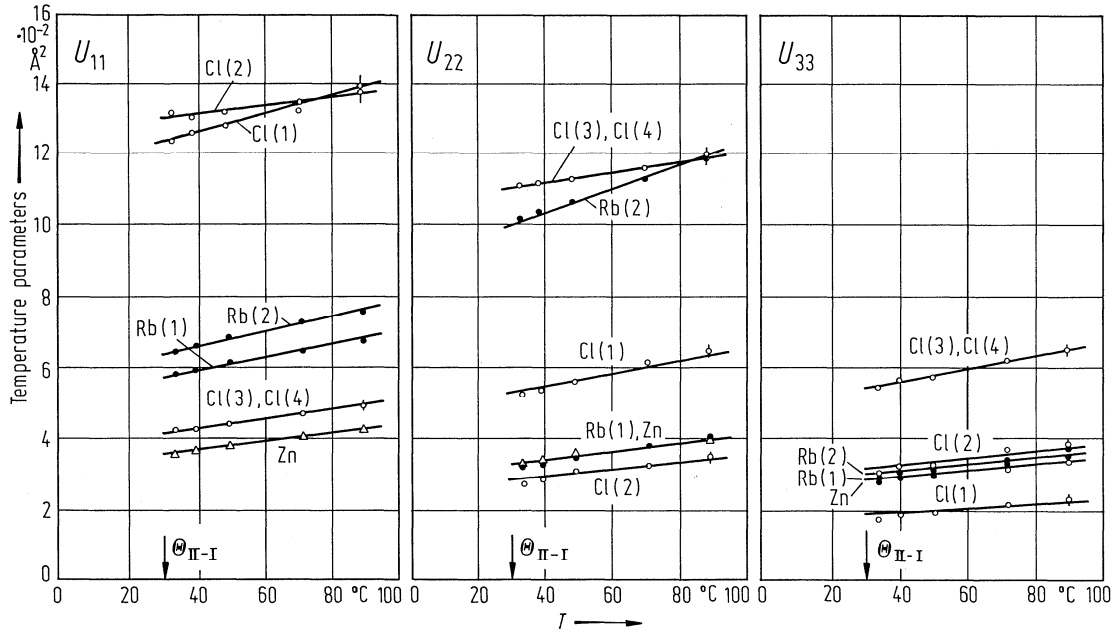

Fig. 39A-10-002. Rb_2ZnCl_4. U_{ij} vs. T [83Ito]. U_{ij}: temperature parameters defined by Eq. (d) in Introduction.

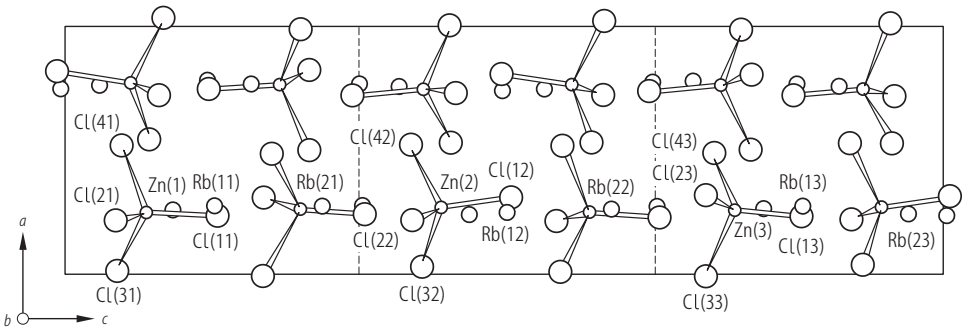

Fig. 39A-10-003. Rb_2ZnCl_4. Crystal structure of phase III [89Ito]. Projection along the *b* axis. $T = 146$ K.

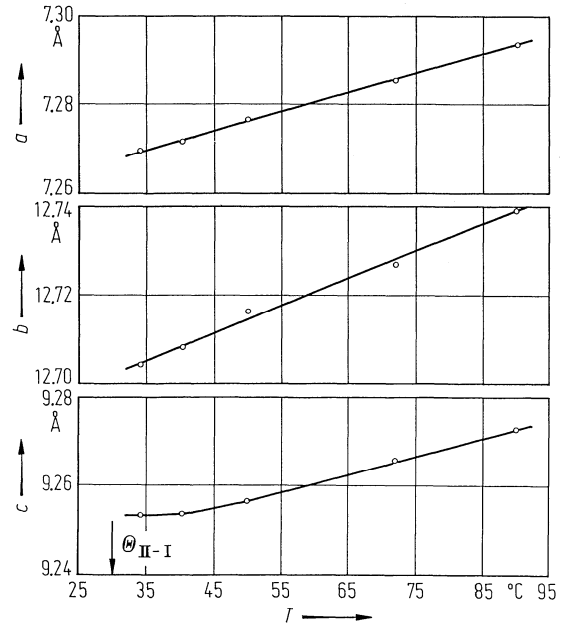

Fig. 39A-10-004. Rb_2ZnCl_4. *a*, *b*, *c* vs. *T* [83Ito]. *a*, *b*, *c*: unit cell parameters.

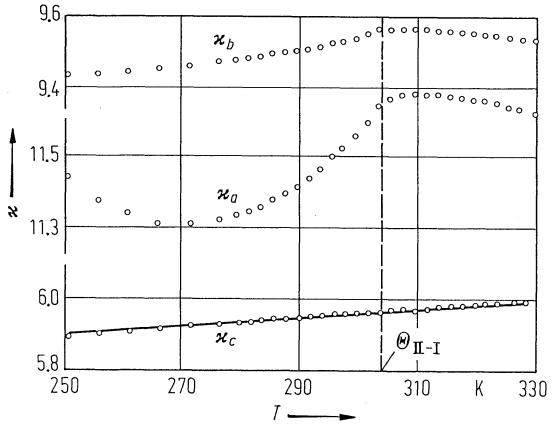

Fig. 39A-10-005. Rb_2ZnCl_4. κ_a, κ_b, κ_c vs. *T* in the vicinity of Θ_{II-I} [81Unr].

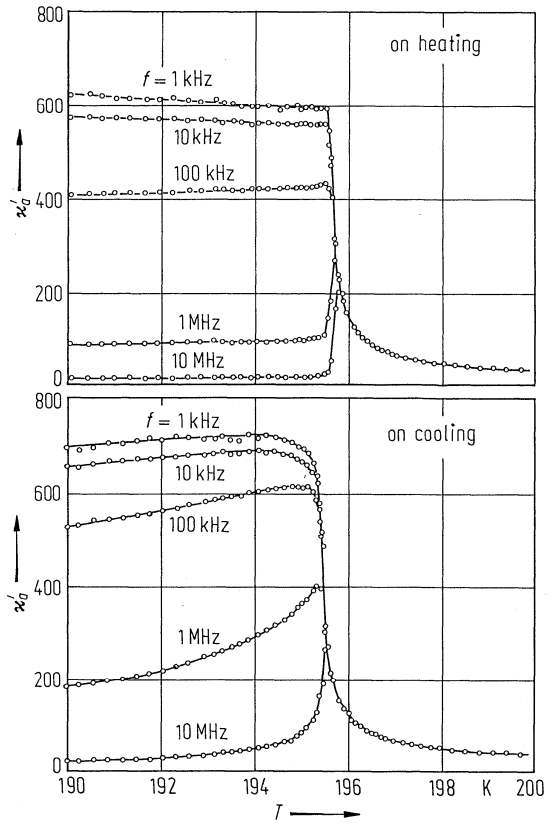

Fig. 39A-10-006. Rb_2ZnCl_4. κ'_a vs. T [85Ham1]. Parameter: f.

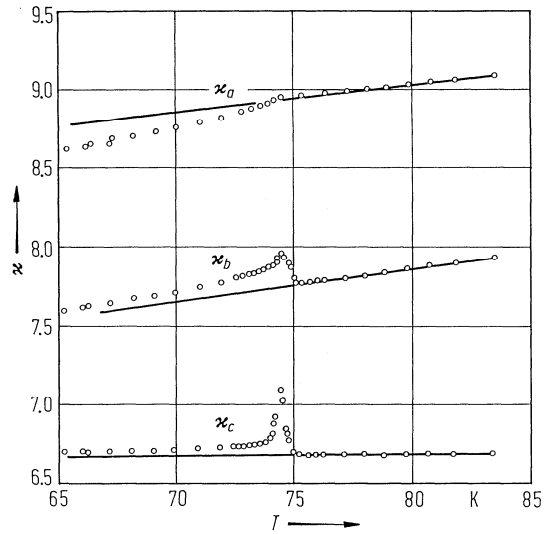

Fig. 39A-10-007. Rb_2ZnCl_4. κ_a, κ_b, κ_c vs. T in the vicinity of Θ_{IV-III} [81Unr].

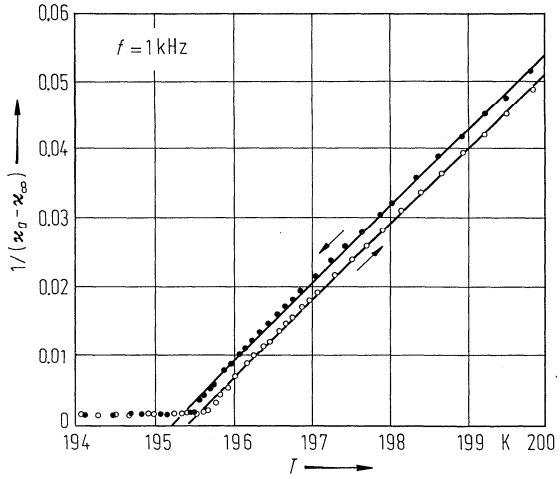

Fig. 39A-10-008. Rb_2ZnCl_4. $1/(\kappa_a - \kappa_\infty)$ vs. T [85Ham1]. The temperature independent part κ_∞ was assumed to be 11.

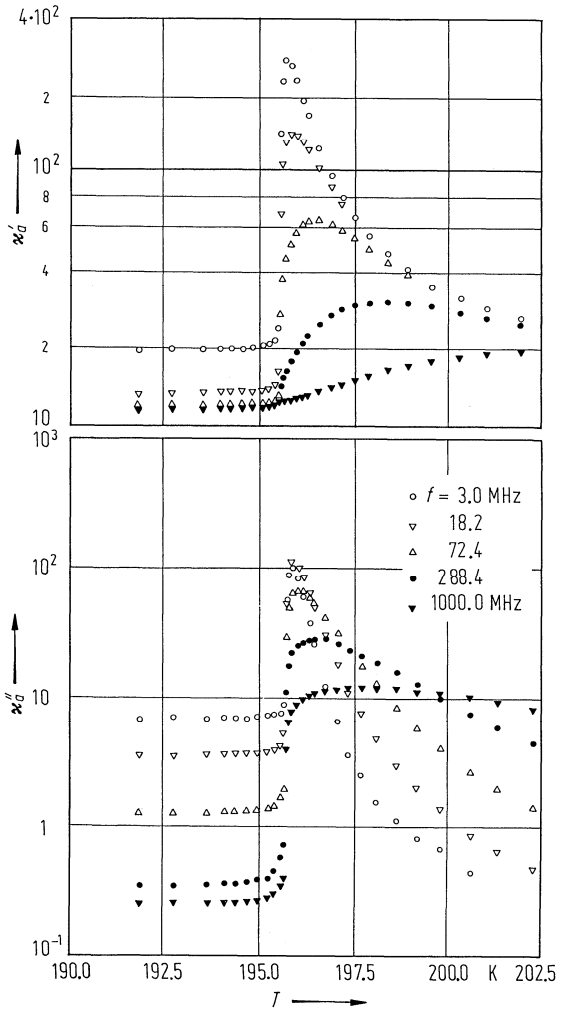

Fig. 39A-10-009. Rb_2ZnCl_4. κ'_a, κ''_a vs. T [84Deg]. Parameter: f.

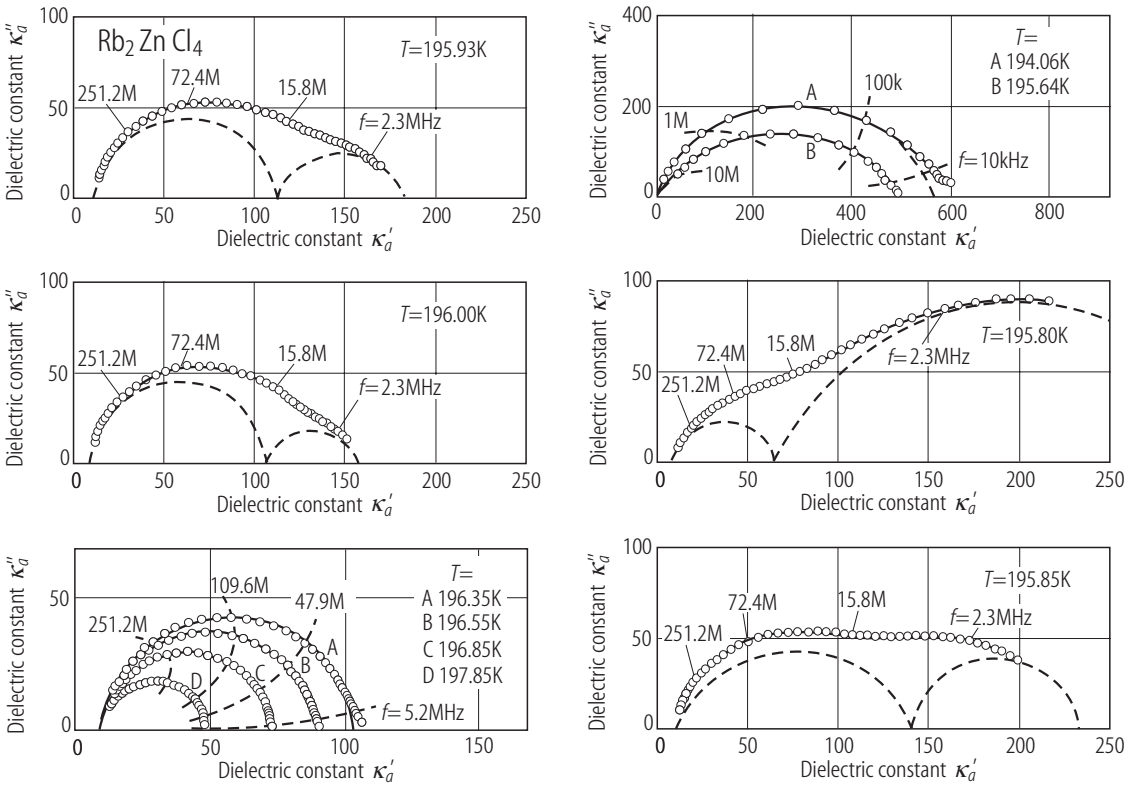

Fig. 39A-10-010. Rb_2ZnCl_4. Cole-Cole diagram of complex dielectric constant [88Ham]. Parameter: *T*. Dielectric dispersion is composed by two relaxations.

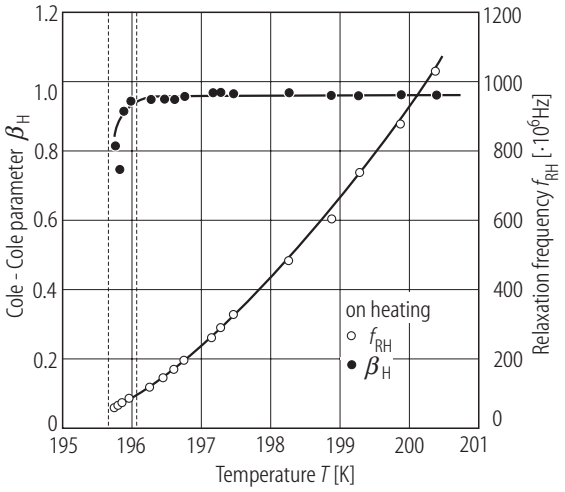

Fig. 39A-10-011. Rb_2ZnCl_4. f_{RH}, β_H vs. *T* [88Ham]. f_{RH}: relaxation frequency of high-frequency dispersion, β_H: Cole-Cole parameter; $\kappa^* = \kappa_\infty + (\kappa_0 - \kappa_\infty)/[1 + (if/f_{RH})^{\beta_H}]$. The temperature region where the low- and high-frequency dispersions coexist is shown by the dotted lines.

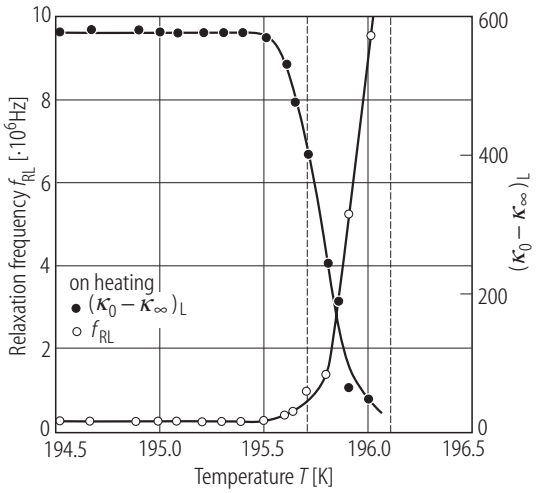

Fig. 39A-10-012. Rb_2ZnCl_4. f_{RL}, $(\kappa_0 - \kappa_\infty)_L$ vs. T in the vicinity of Θ_f [88Ham]. f_{RL}, $(\kappa_0 - \kappa_\infty)_L$: relaxation frequency and oscillator strength of the low-frequency dispersion. Dotted lines indicate the coexistence temperature region of low- and high-frequency dispersions.

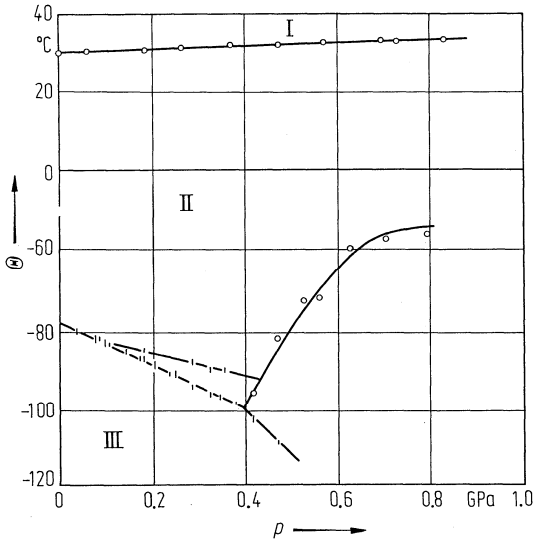

Fig. 39A-10-013. Rb_2ZnCl_4. Θ vs. p [85Ges].

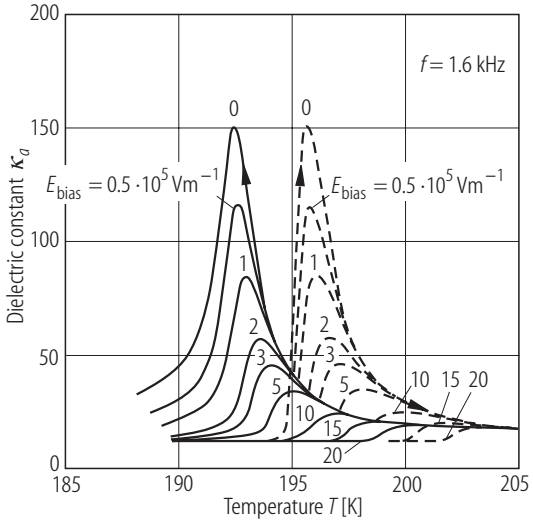

Fig. 39A-10-014. Rb_2ZnCl_4. κ_a vs. T [88Fou]. Parameter: E_{bias}. Full lines: on cooling; broken lines: on heating.

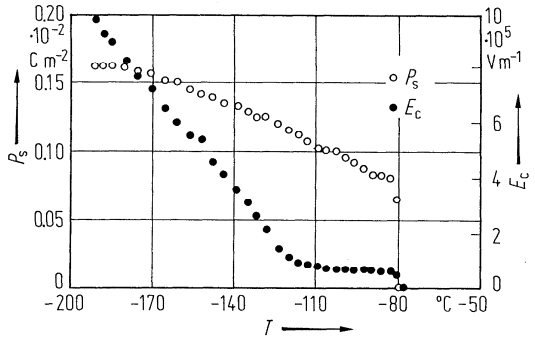

Fig. 39A-10-015. Rb_2ZnCl_4. P_s, E_c vs. T [77Saw].

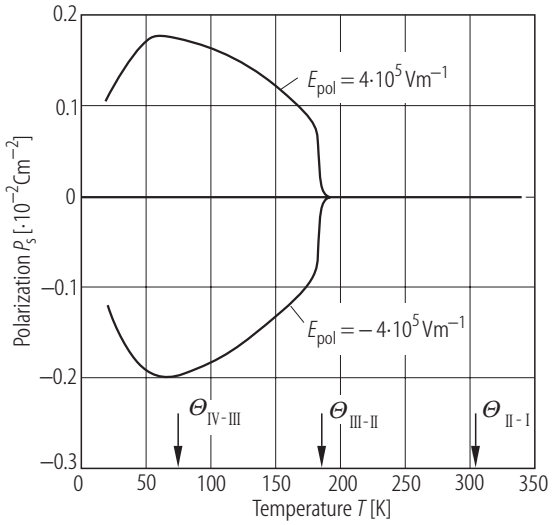

Fig. 39A-10-016. Rb_2ZnCl_4. P_s vs. T [81Wad]. Obtained from pyroelectric charge measurements. E_{pol}: poling field.

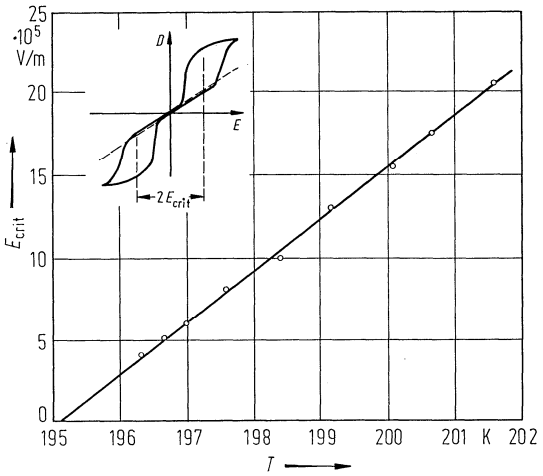

Fig. 39A-10-017. Rb_2ZnCl_4. E_{crit} vs. T [81Unr]. E_{crit} is defined in the insert.

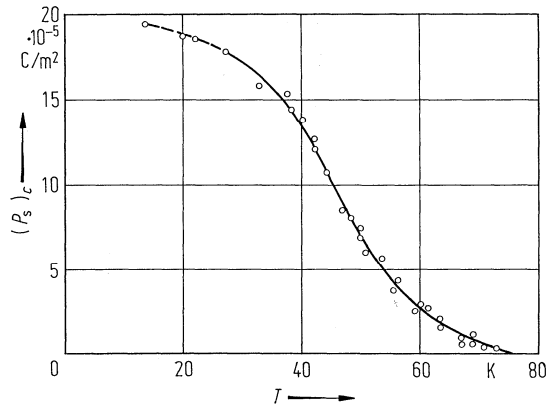

Fig. 39A-10-018. Rb_2ZnCl_4. $(P_s)_c$ vs. T [81Unr]. $(P_s)_c$: component of P_s along the c axis.

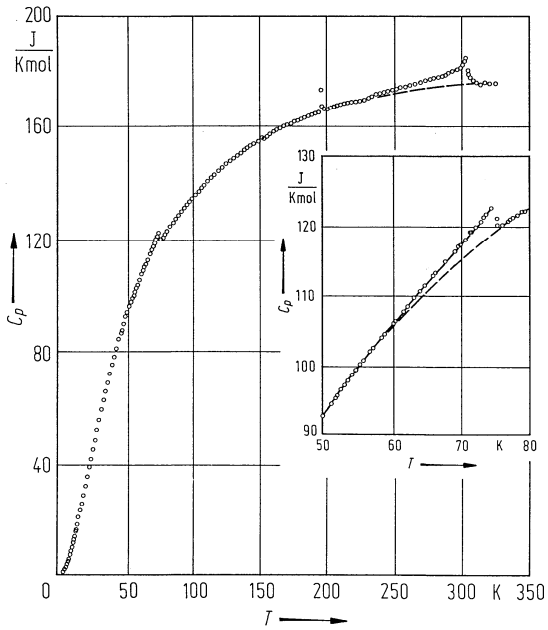

Fig. 39A-10-019. Rb_2ZnCl_4. C_p vs. T [83Ata]. C_p: molar heat capacity at constant pressure.

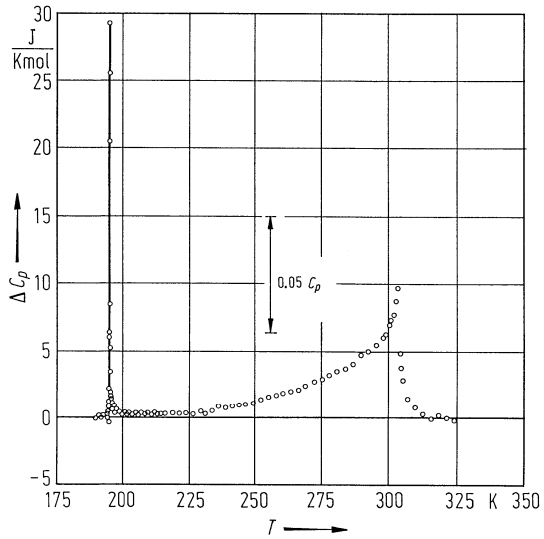

Fig. 39A-10-020. Rb_2ZnCl_4. ΔC_p vs. T [83Ata]. ΔC_p: excess molar heat capacity at constant pressure.

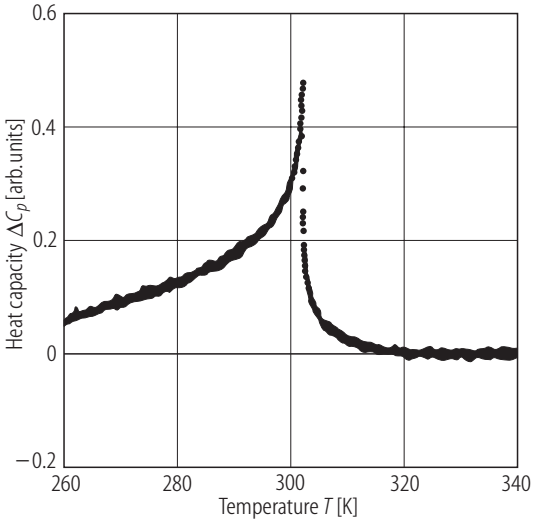

Fig. 39A-10-021. Rb_2ZnCl_4. ΔC_p vs. T [94Hag]. ΔC_p: excess heat capacity at constant pressure. ac calorimetric method.

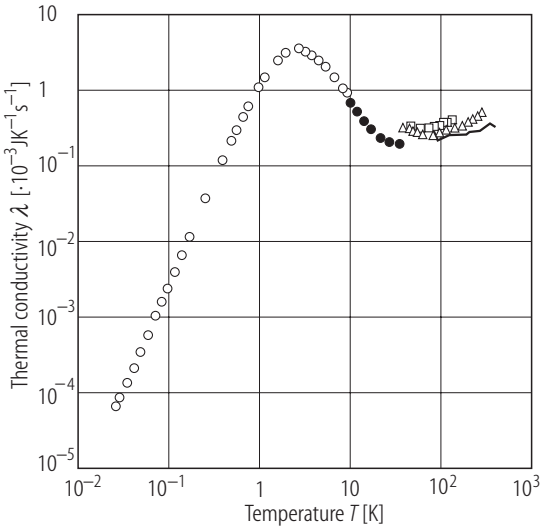

Fig. 39A-10-022. Rb_2ZnCl_4. λ vs. T [94Zhu]. λ: thermal conductivity along the polar a axis. Solid line: [89Str]. Different marks distinguish the data for different specimens with different methods. Open circle: superconducting Nb wire, dilution refrigerator with carbon thermometer. Full circle: Cu wire, dilution refrigerator with carbon thermometer. Square and triangle: Cu wire, He cryostat with Pt thermometer.

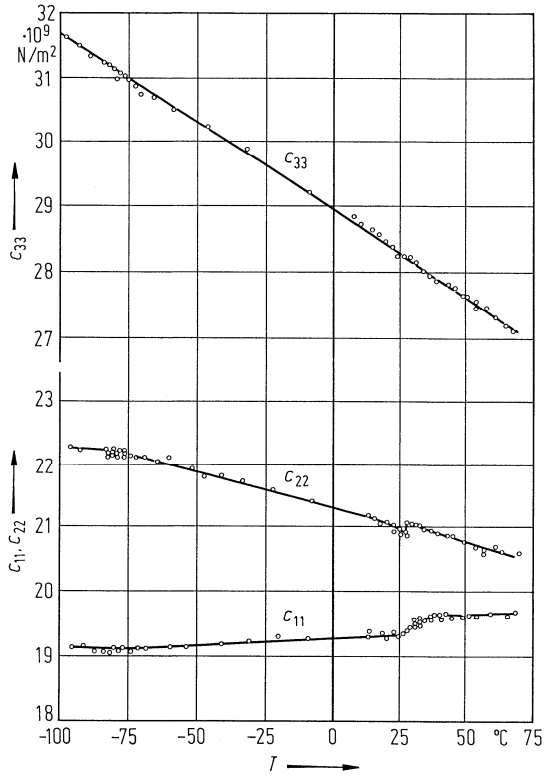

Fig. 39A-10-023. Rb_2ZnCl_4. c_{11}, c_{22}, c_{33} vs. T [82Lus]. Brillouin scattering. $\lambda = 514.5$ nm.

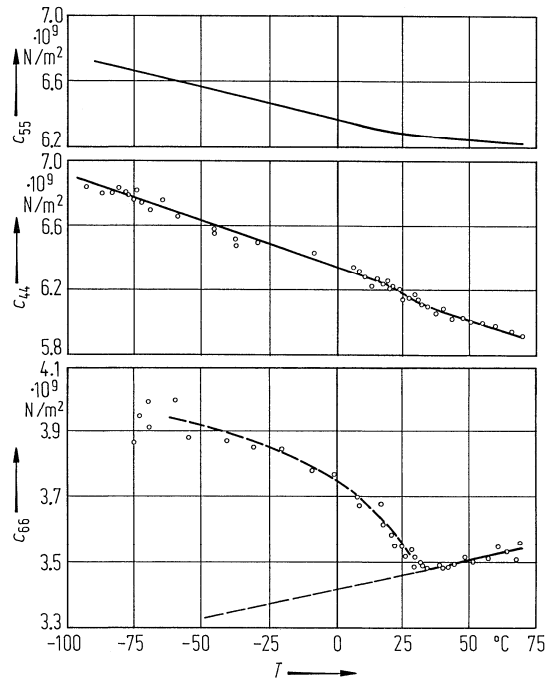

Fig. 39A-10-024. Rb_2ZnCl_4. c_{44}, c_{55}, c_{66} vs. T [82Lus]. Brillouin scattering. $\lambda = 514.5$ nm. c_{55} was calculated from $(c_{44} + c_{66})/2$.

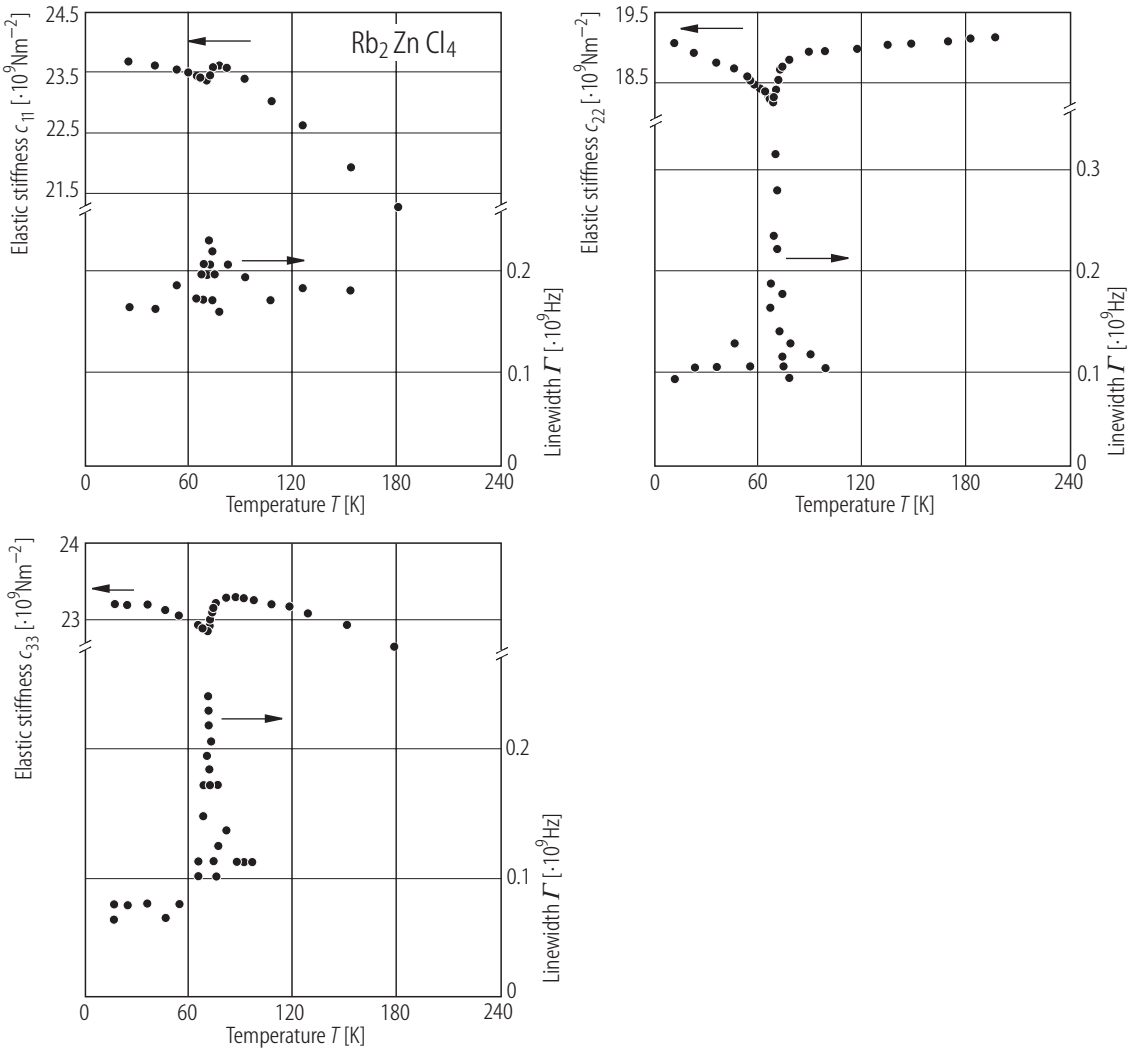

Fig. 39A-10-025. Rb_2ZnCl_4. $c_{\lambda\lambda}$, Γ vs. T [90Qui]. Γ: full width at half maximum of Brillouin lines. $\lambda = 514.5$ nm.

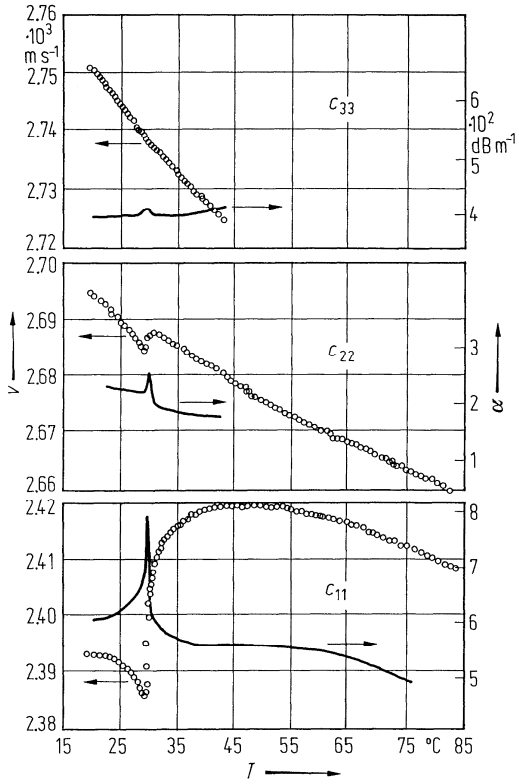

Fig. 39A-10-026. Rb_2ZnCl_4. υ vs. T, α vs. T [79Hir]. υ: sound velocity of $c_{\lambda\lambda}$ longitudinal mode, α: attenuation. f = 10 MHz.

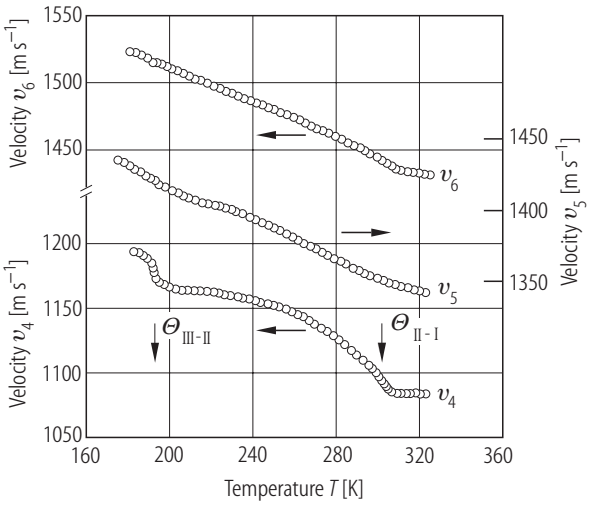

Fig. 39A-10-027. Rb_2ZnCl_4. υ_λ vs. T [93Kit]. υ_λ: sound velocity of $c_{\lambda\lambda}$ shear mode. f = 10 MHz.

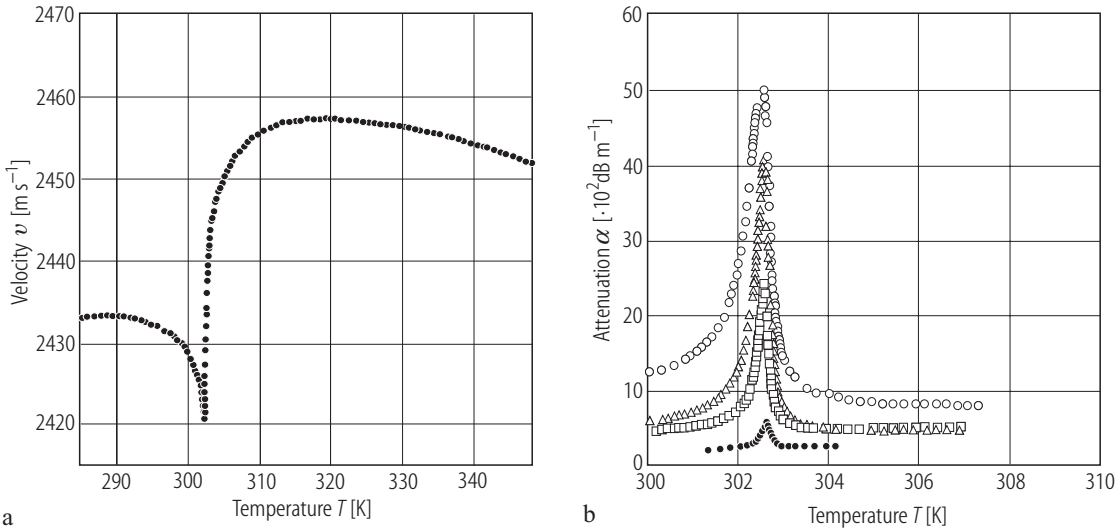

Fig. 39A-10-028. Rb_2ZnCl_4. (**a**) v vs. T, (**b**) α vs. T [90Hu]. v, α: velocity and attenuation of the longitudinal c_{11} mode. (**a**) f = 10 MHz. (**b**) full circle: f = 10 MHz, open square: 30 MHz, open triangle: 50 MHz, open circle: 70 MHz.

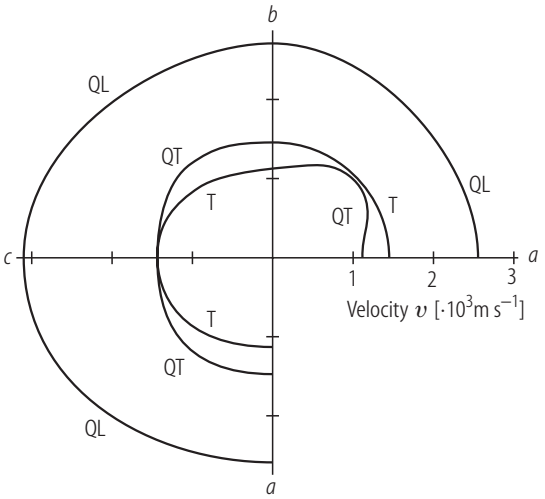

Fig. 39A-10-029. Rb_2ZnCl_4. Polar diagram of v, the acoustic phonon velocity [89Hor]. Brillouin scattering. QL, QT and T indicate quasilongitudinal, quasitransverse and transverse phonon modes, respectively. On the axes the QL modes turn strictly longitudinal. T = 300 K.

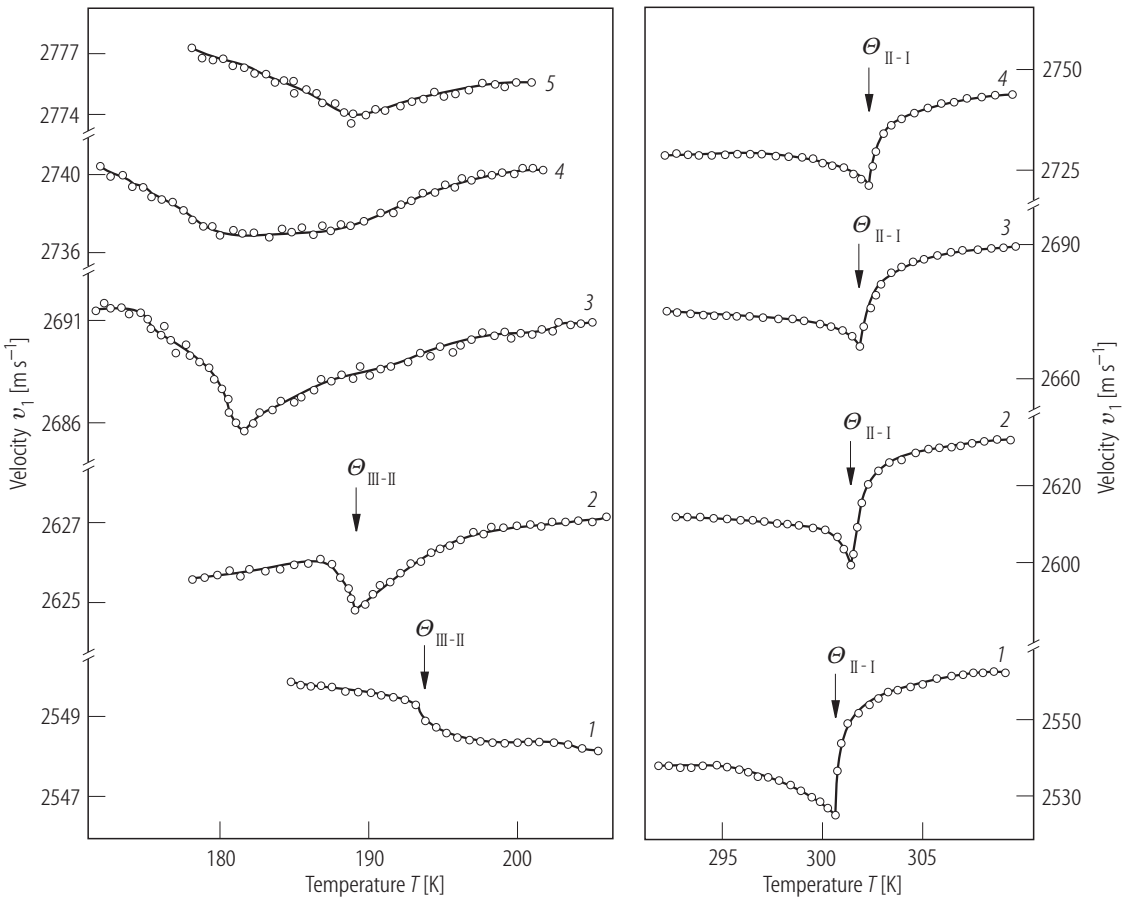

Fig. 39A-10-030. Rb_2ZnCl_4. v_1 vs. T [93Kit]. v_1: velocity of the longitudinal sound wave propagating along the [100] direction. f = 10 MHz. Parameter: *p. 1*: $p = 1 \cdot 10^5$ Pa, *2*: $1.65 \cdot 10^8$ Pa, *3*: $2.75 \cdot 10^8$ Pa, *4*: $3.70 \cdot 10^8$ Pa, *5*: $4.35 \cdot 10^8$ Pa.

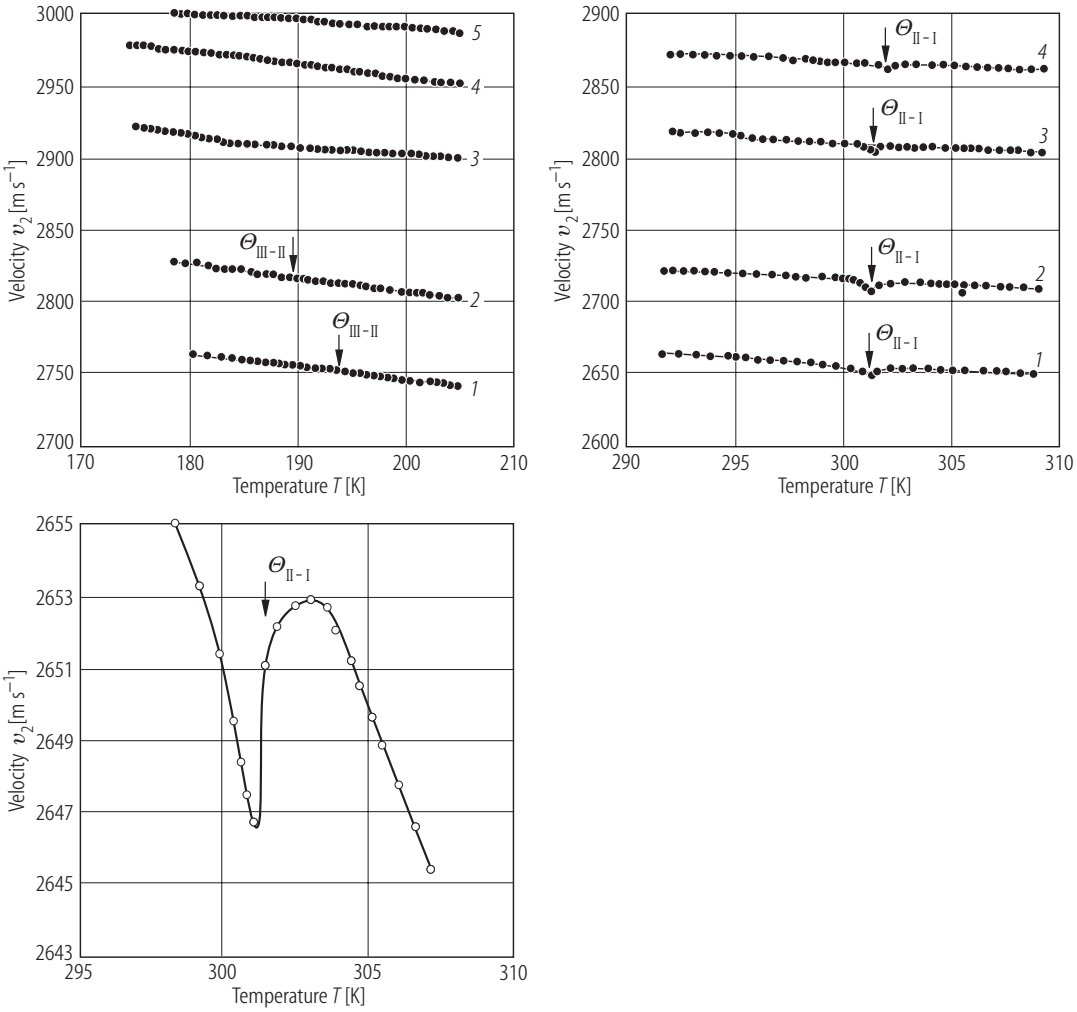

Fig. 39A-10-031. Rb_2ZnCl_4. v_2 vs. T [93Kit]. v_2: velocity of the longitudinal sound wave propagating along the [010] direction. f = 10 MHz. Parameter: p. *1*: $p = 1 \cdot 10^5$ Pa, *2*: $1.25 \cdot 10^8$ Pa, *3*: $2.75 \cdot 10^8$ Pa, *4*: $3.75 \cdot 10^8$ Pa, *5*: $4.35 \cdot 10^8$ Pa. Lower figure: v_2 vs. T near Θ_{II-I} at $p = 1 \cdot 10^5$ Pa.

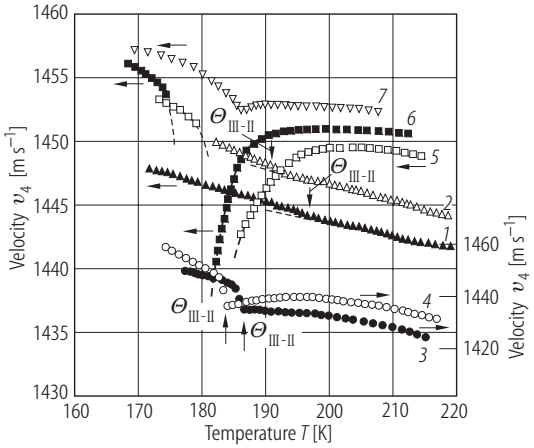

Fig. 39A-10-032. Rb_2ZnCl_4. v_4 vs. T [93Kit]. v_4: velocity of the transverse sound of the c_{44} mode. f = 10 MHz. Parameter: p. *1*: $p = 1 \cdot 10^5$ Pa, *2*: $9.0 \cdot 10^7$ Pa, *3*: $1.95 \cdot 10^8$ Pa, *4*: $2.25 \cdot 10^8$ Pa, *5*: $2.75 \cdot 10^8$ Pa, *6*: $3.75 \cdot 10^8$ Pa, *7*: $4.30 \cdot 10^8$ Pa.

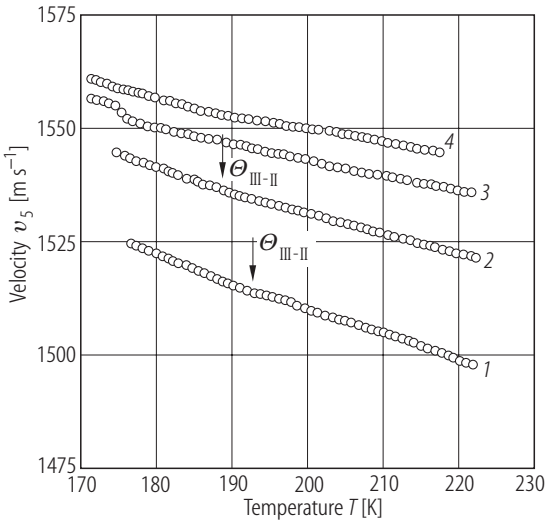

Fig. 39A-10-033. Rb_2ZnCl_4. v_5 vs. T [93Kit]. v_5: velocity of the transverse sound of the c_{55} mode. f = 10 MHz. Parameter: *p. 1*: $p = 1 \cdot 10^5$ Pa, *2*: $1.75 \cdot 10^8$ Pa, *3*: $3.25 \cdot 10^8$ Pa, *4*: $4.35 \cdot 10^8$ Pa.

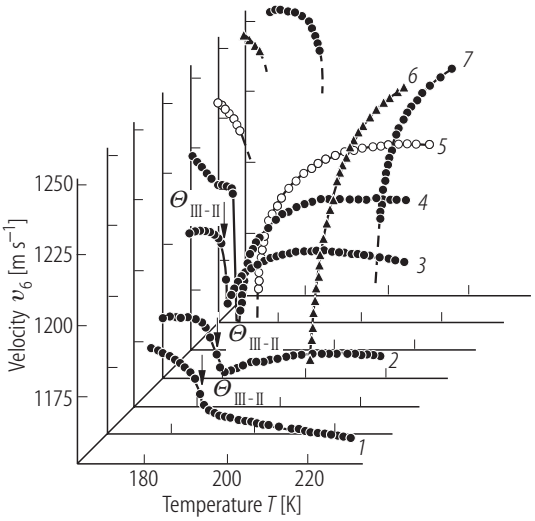

Fig. 39A-10-034. Rb_2ZnCl_4. v_6 vs. T [93Kit]. v_6: velocity of the transverse sound of the c_{66} mode. f = 10 MHz. Parameter: *p. 1*: $p = 1 \cdot 10^5$ Pa, *2*: $9.5 \cdot 10^7$ Pa, *3*: $1.75 \cdot 10^8$ Pa, *4*: $2.25 \cdot 10^8$ Pa, *5*: $2.75 \cdot 10^8$ Pa, *6*: $3.75 \cdot 10^8$ Pa, *7*: $4.35 \cdot 10^8$ Pa.

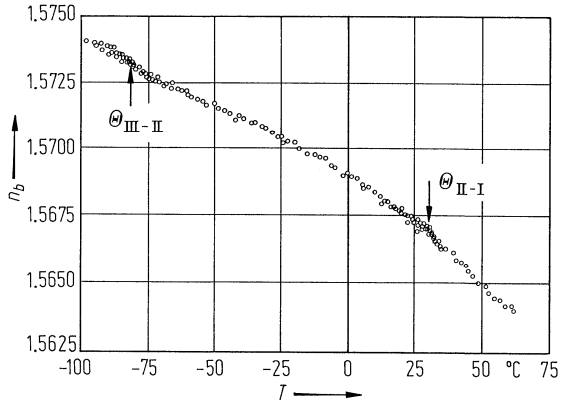

Fig. 39A-10-035. Rb_2ZnCl_4. n_b vs. T [82Yam]. $\lambda = 488.0$ nm.

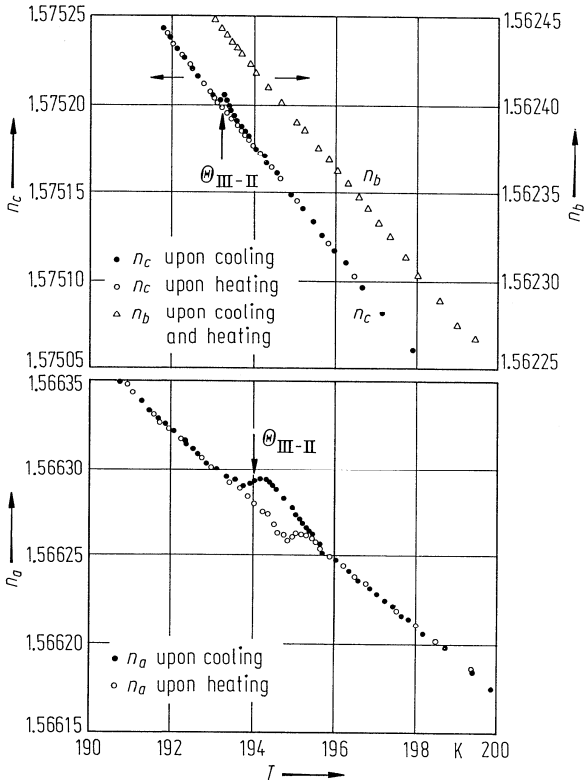

Fig. 39A-10-036. Rb_2ZnCl_4. n_a, n_b, n_c vs. T in the vicinity of Θ_{III-II} [85San2]. $\lambda = 633$ nm.

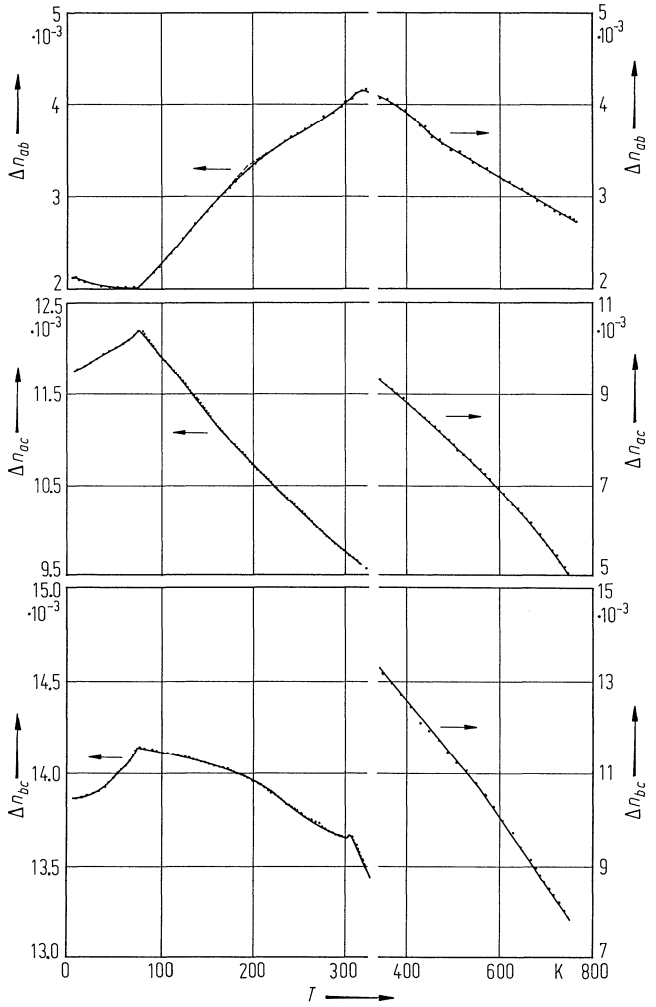

Fig. 39A-10-037. Rb_2ZnCl_4. Δn_{ab}, Δn_{ac}, Δn_{bc} vs. T [82Gun]. $\lambda = 633$ nm.

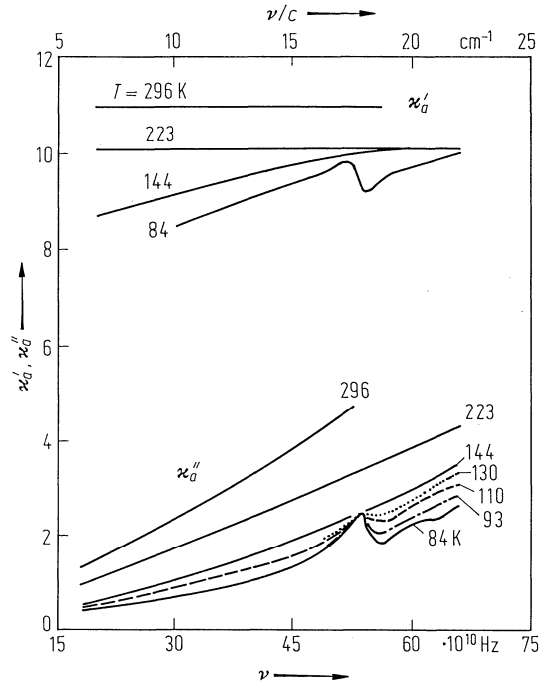

Fig. 39A-10-038. Rb_2ZnCl_4. κ'_a, κ''_a vs. ν [82Pet]. Parameter: *T*.

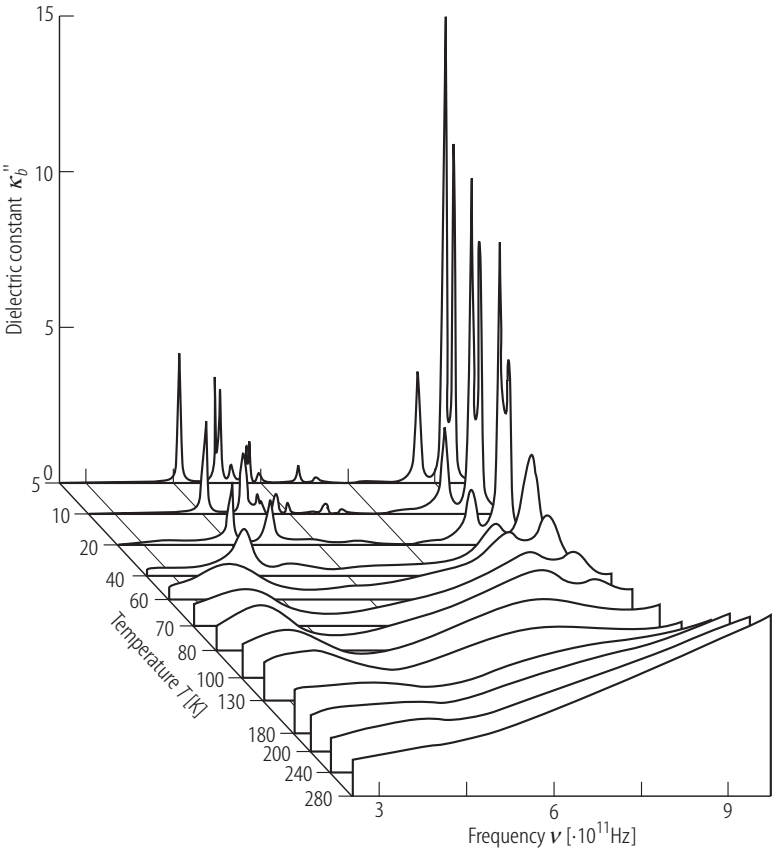

Fig. 39A-10-039. Rb_2ZnCl_4. κ''_b vs. ν [90Vol]. Parameter: *T*.

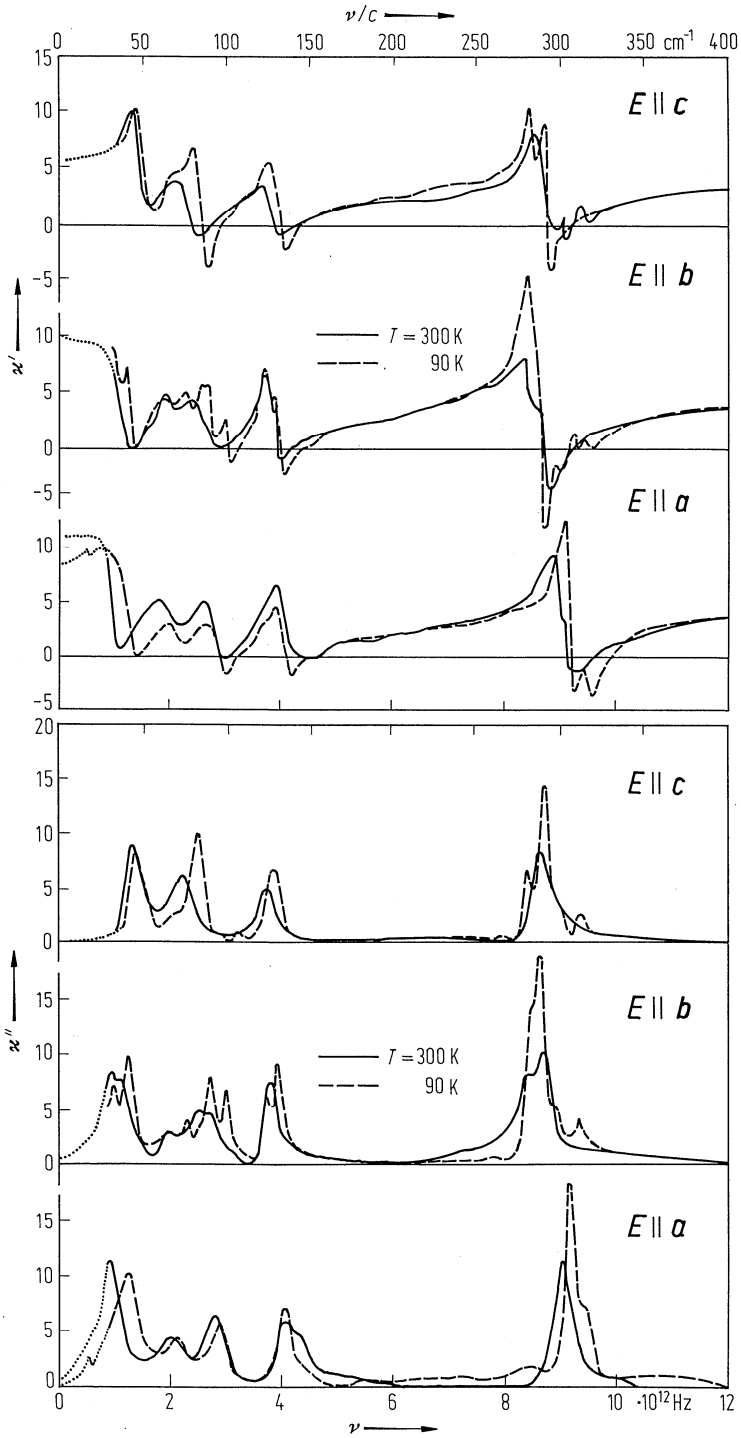

Fig. 39A-10-040. Rb_2ZnCl_4. κ', κ'' vs. ν [82Pet]. Parameter: T. The curves were obtained from reflectivity data using Kramers-Kronig relation.

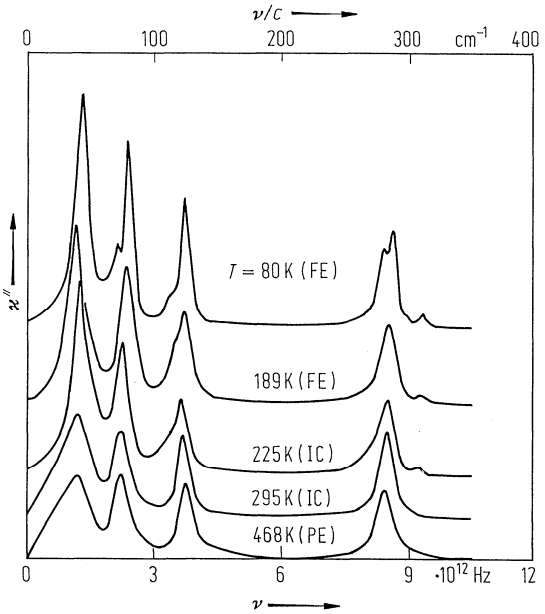

Fig. 39A-10-041. Rb_2ZnCl_4. κ'' vs. ν [84Ech]. Parameter: T. κ'': imaginary part of the dielectric constant obtained from the infrared reflection spectra with $\boldsymbol{E} \parallel \boldsymbol{a}$. FE, IC and PE in the parentheses denote ferroelectric, incommensurate and paraelectric phase, respectively.

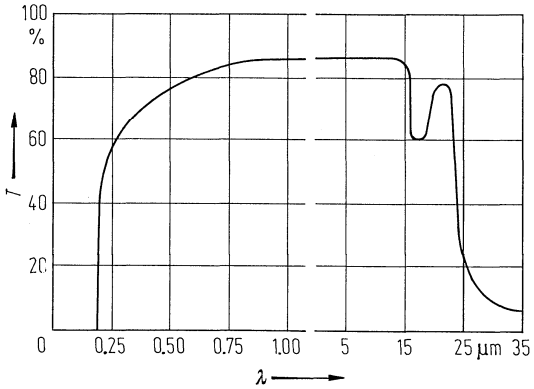

Fig. 39A-10-042. Rb_2ZnCl_4. T vs. λ [82Gun]. T: transmission. Sample thickness is 0.88 mm.

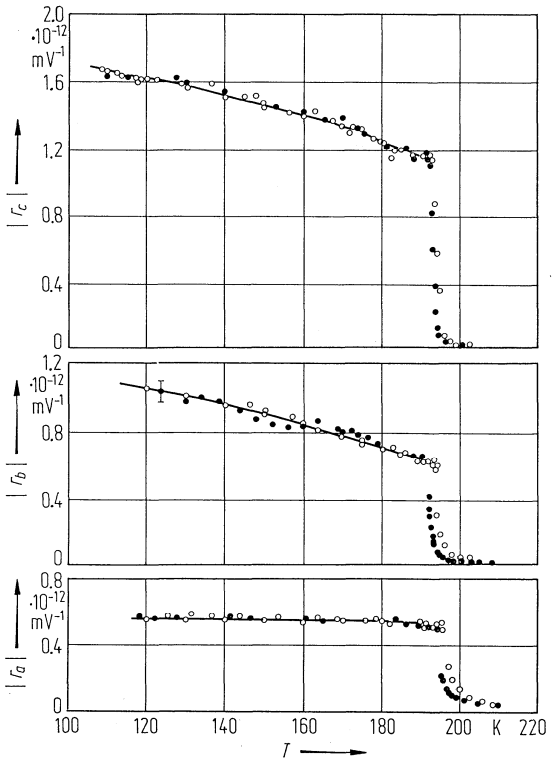

Fig. 39A-10-043. Rb_2ZnCl_4. $|r_a|$, $|r_b|$, $|r_c|$ vs. T [84San]. r_a, r_b, r_c: electrooptic coefficients for light propagation along the a, b and c axes. $|r_a| = |r_{31} - (n_2/n_3)^3 r_{21}|$, $|r_b| = |r_{11} - (n_3/n_1)^3 r_{31}|$, $|r_c| = |r_{11} - (n_2/n_1)^3 r_{21}|$. $r_{\lambda i}$: electrooptic tensor component. $\lambda = 633$ nm. Open circle: on heating, full circle: on cooling.

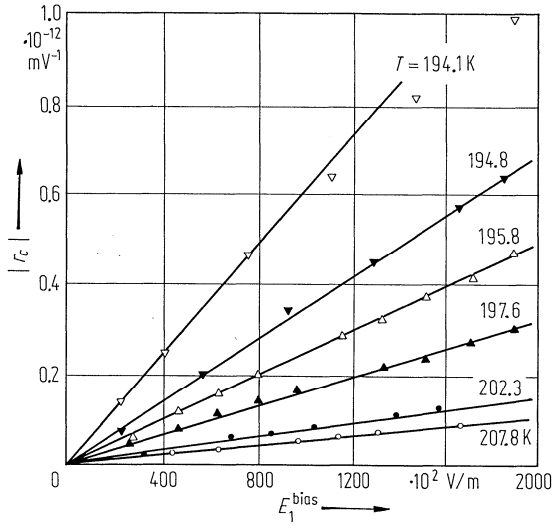

Fig. 39A-10-044. Rb_2ZnCl_4. $|r_c|$ vs. E_1^{bias} [84San]. Parameter: T. $|r_c| = |r_{11} - (n_2/n_1)^3 r_{21}|$. $\lambda = 632.8$ nm. E_1^{bias}: E_{bias} along the a axis.

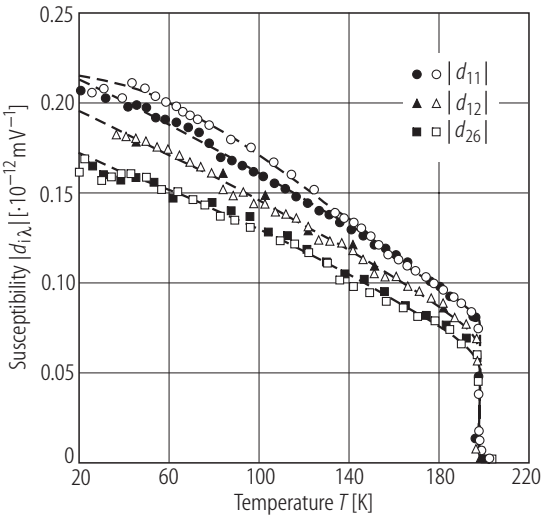

Fig. 39A-10-045. Rb_2ZnCl_4. $|d_{i\lambda}|$ vs. T [90Bas]. $d_{i\lambda}$: nonlinear optical susceptibility. $\lambda = 1064$ nm. Open symbols: on heating, full symbols: on cooling.

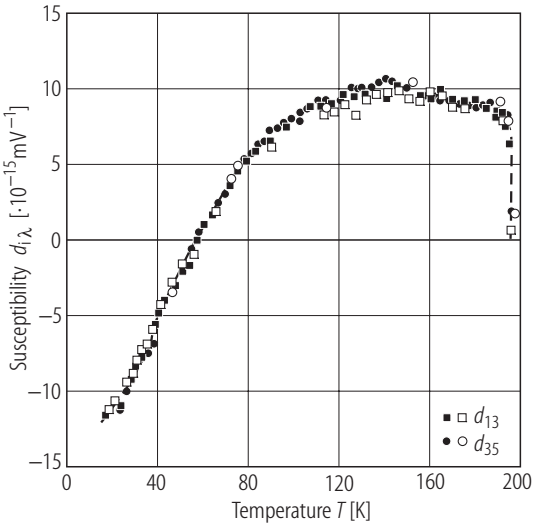

Fig. 39A-10-046. Rb_2ZnCl_4. $d_{i\lambda}$ vs. T [90Bas]. $d_{i\lambda}$: nonlinear optical susceptibility. $\lambda = 1064$ nm. The signs of $d_{i\lambda}$ are relative ones with respect to d_{11}. Open symbols: on heating, full symbols: on cooling.

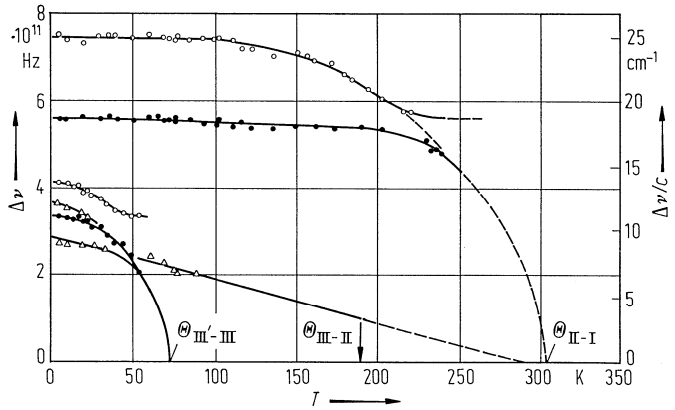

Fig. 39A-10-047. Rb_2ZnCl_4. $\Delta\nu$ vs. T [81Wad]. $\Delta\nu$: Raman shift of soft modes.

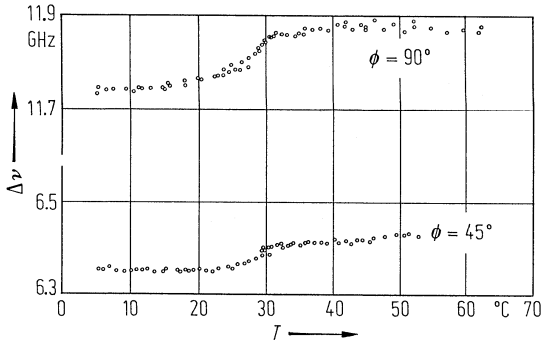

Fig. 39A-10-048. Rb_2ZnCl_4. $\Delta\nu$ vs. T [81Yam]. $\Delta\nu$: Brillouin frequency shift for c_{11} mode. ϕ: scattering angle. $\lambda = 488$ nm.

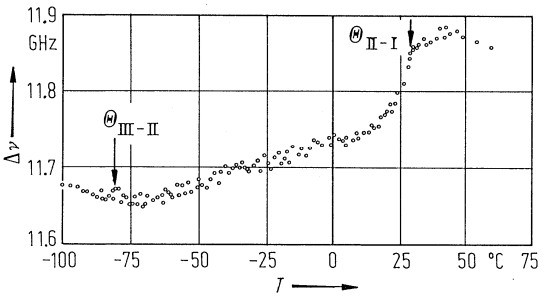

Fig. 39A-10-049. Rb_2ZnCl_4. $\Delta\nu$ vs. T [82Yam]. $\Delta\nu$: Brillouin frequency shift for c_{11} mode. $\lambda = 488$ nm.

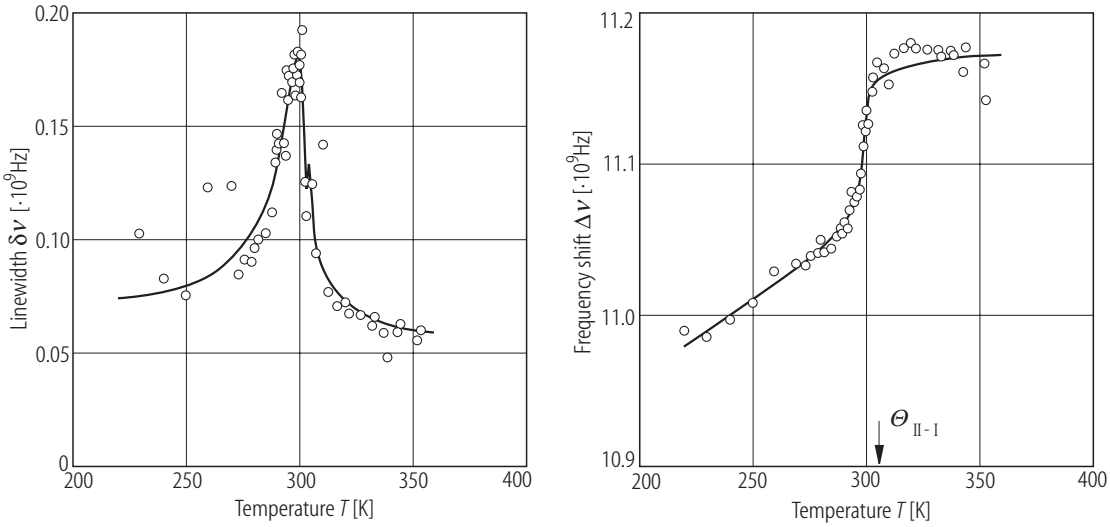

Fig. 39A-10-050. Rb_2ZnCl_4. $\Delta\nu$, $\delta\nu$ of c_{11} mode vs. T [89Hor]. $\Delta\nu$: Brillouin frequency shift, $\delta\nu$: half width at half maximum of Brillouin line. $XY(ZZ)\overline{X}Y$ scattering geometry. $\lambda = 514.5$ nm.

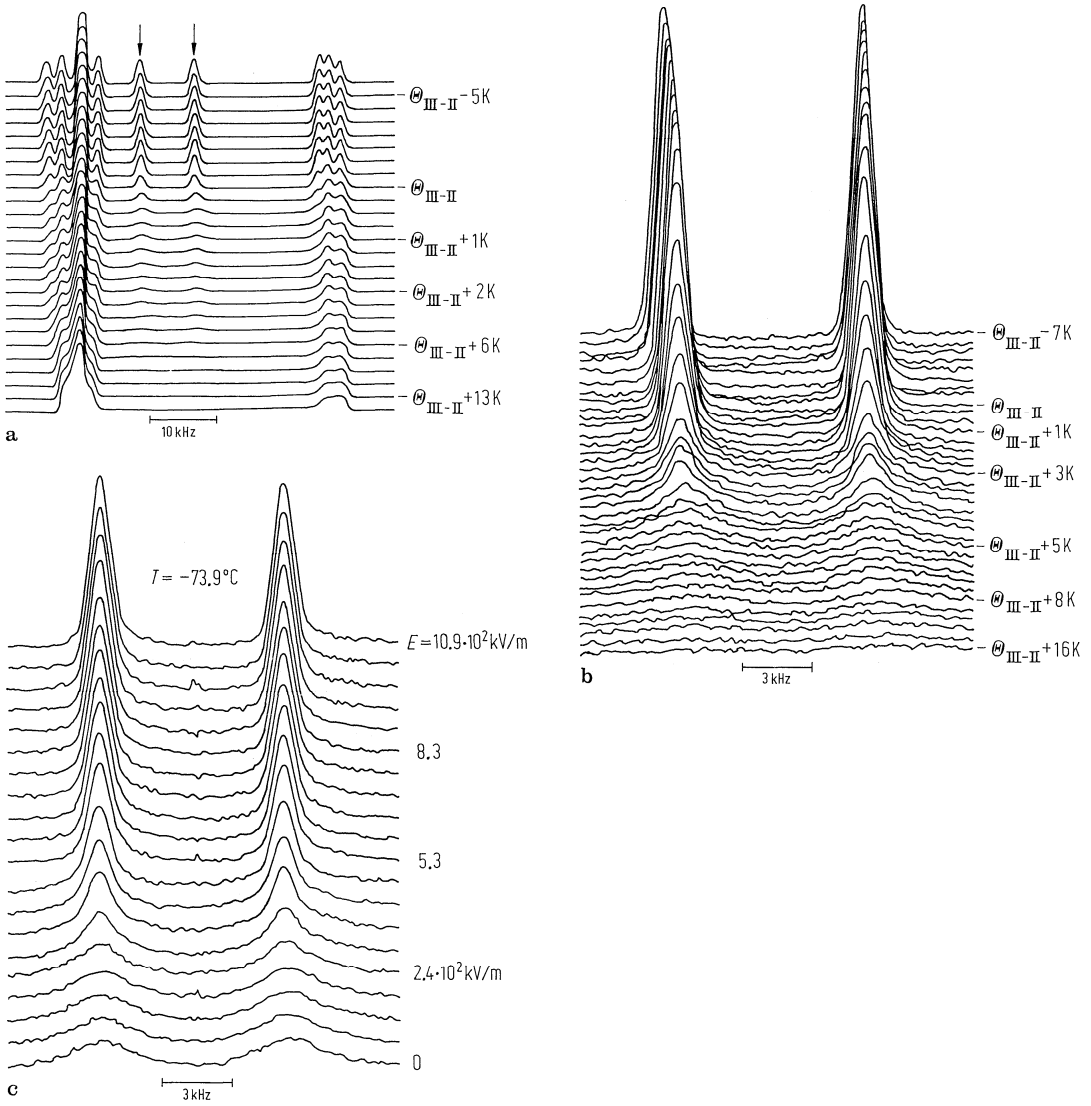

Fig. 39A-10-051. Rb_2ZnCl_4. (**a**) ^{87}Rb 1/2 ↔ –1/2 central transition lineshape near $\Theta_{III–II}$ [85Pet]. Parameter: T. $\boldsymbol{H} \perp \boldsymbol{b}$, $\angle(\boldsymbol{H}, \boldsymbol{c}) = 27°$. (**b**) Close-up view around the two lines indicated by arrows in (**a**). (**c**) Dependence of the two lines on applied electric field E along the a axis. $T = –73.9$ °C.

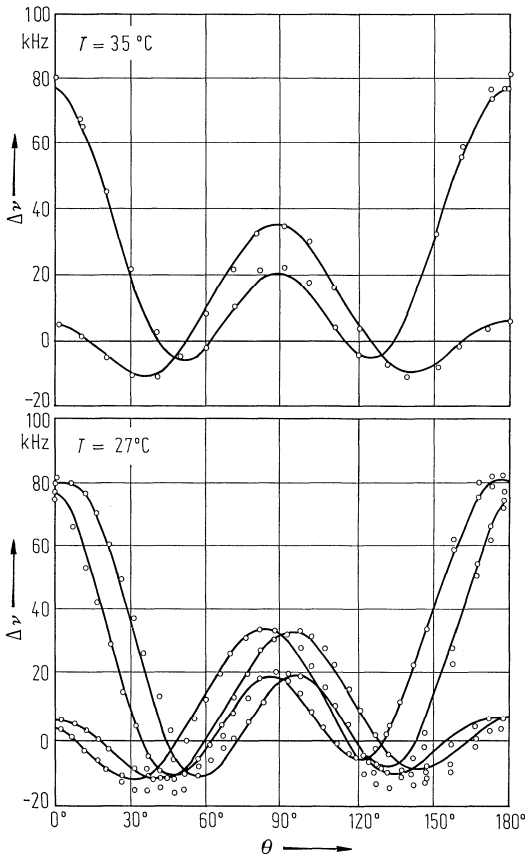

Fig. 39A-10-052. Rb_2ZnCl_4. $\Delta\nu$ vs. θ [81Rut]. $\Delta\nu$: second-order quadrupole shift of the ^{87}Rb $1/2 \leftrightarrow -1/2$ transition. θ: the angle between $\boldsymbol{H}$ and b axis in the a–b plane. $\boldsymbol{H} \perp \boldsymbol{c}$.

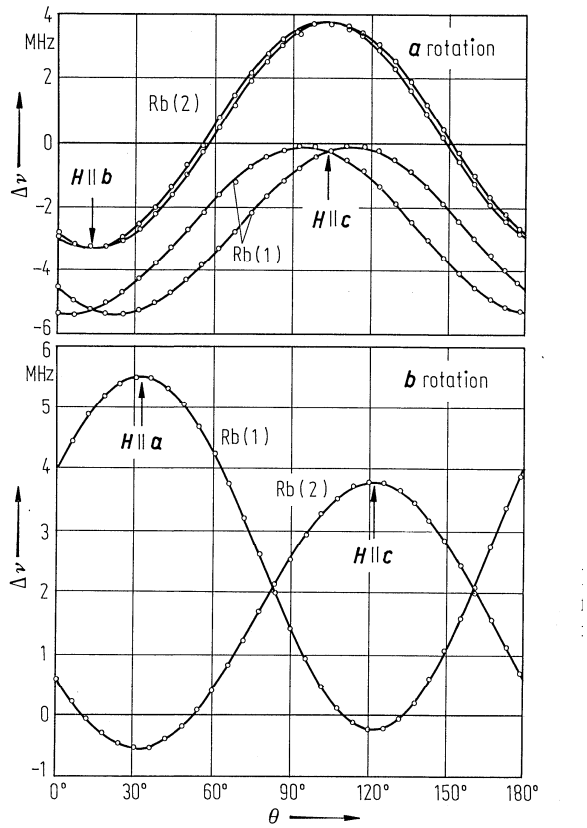

Fig. 39A-10-053. Rb_2ZnCl_4. $\Delta\nu$ vs. θ [82Sch]. $\Delta\nu$: ^{87}Rb satellite line splitting. ν_L = 98.17 MHz. $T \approx 34$ °C.

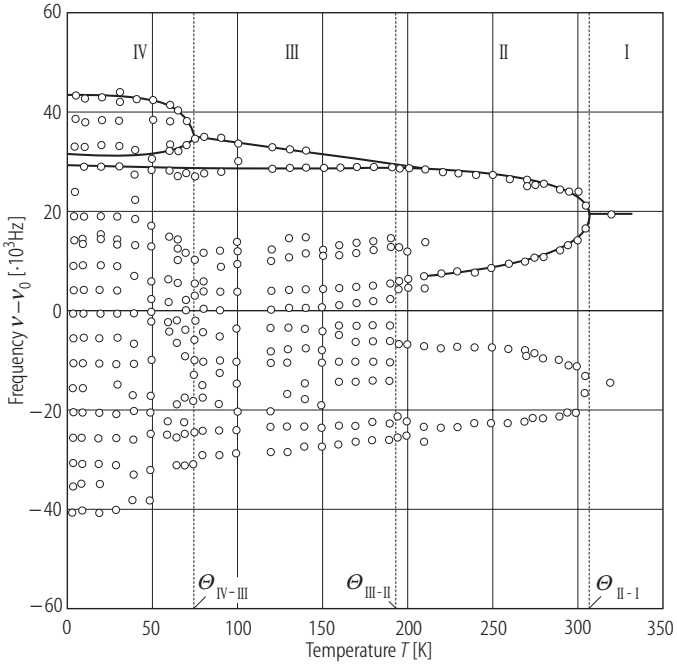

Fig. 39A-10-054. Rb_2ZnCl_4. $\nu - \nu_0$ vs. T [92Api]. ν: ^{87}Rb 1/2 → −1/2 NMR transition frequencies. ν_0: central frequency. $\boldsymbol{H}_0 \perp \boldsymbol{b}$, $\angle(\boldsymbol{H}_0, \boldsymbol{c}) = 122°$.

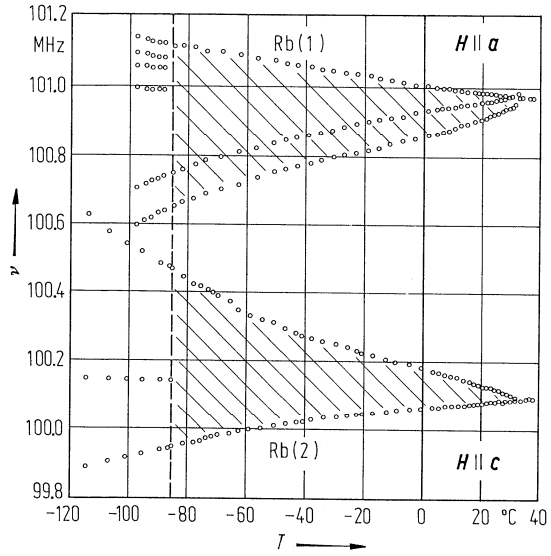

Fig. 39A-10-055. Rb_2ZnCl_4. ν vs. T [82Sch]. ν: NMR resonance frequency of ^{87}Rb upper satellite transition. Hatched region denotes incommensurate continuous spectra.

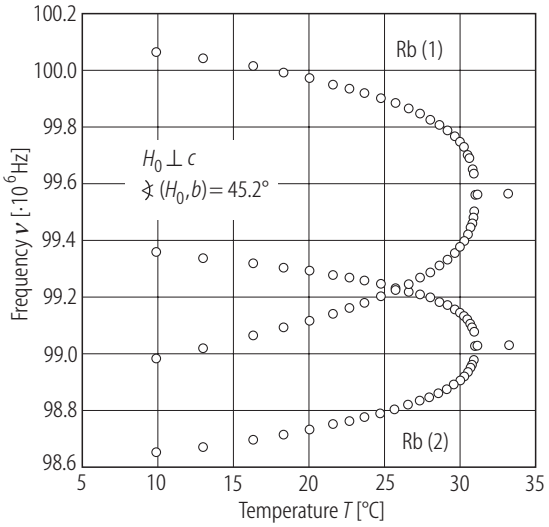

Fig. 39A-10-056. Rb_2ZnCl_4. ν vs. T [89Wal]. ν: NMR resonance frequency of the intensity maxima (edge singularities in phase II) of the ^{87}Rb upper frequency satellite transition.

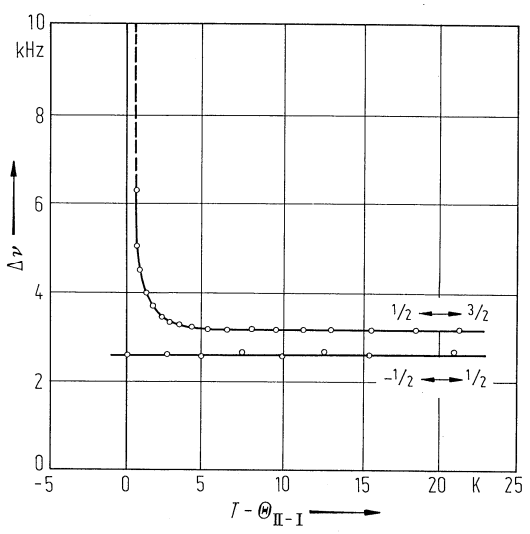

Fig. 39A-10-057. Rb_2ZnCl_4. $\Delta\nu$ vs. $T - \Theta_{II-I}$ [82Bli]. $\Delta\nu$: half-widths of the $^{87}Rb(1)$ NMR $1/2 \leftrightarrow 3/2$ satellite and the $1/2 \leftrightarrow -1/2$ central lines. $\nu_L = 88.12$ MHz. $\boldsymbol{H} \perp \boldsymbol{b}$, $\angle(\boldsymbol{H}, \boldsymbol{c}) = 43°$.

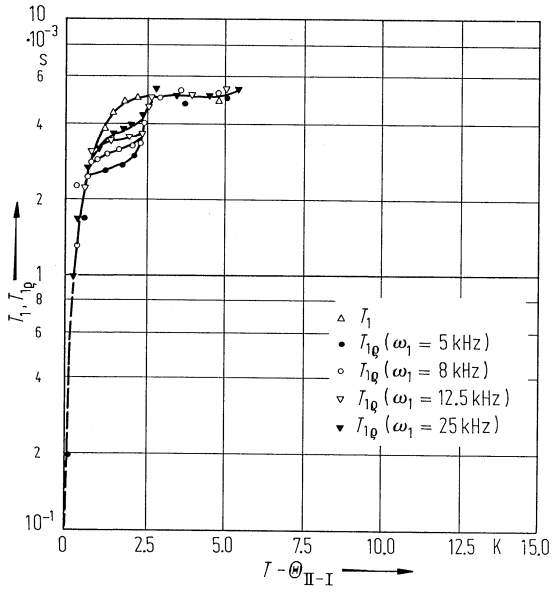

Fig. 39A-10-058. Rb_2ZnCl_4. T_1, $T_{1\rho}$ vs. $T - \Theta_{II-I}$ [82Bli]. Parameter: angular frequency ω_1 in the rotating frame. $^{87}Rb(2)$ $1/2 \leftrightarrow 3/2$ transition. $\nu_L = 88.12$ MHz. $\boldsymbol{H} \perp \boldsymbol{b}$, $\angle(\boldsymbol{H}, \boldsymbol{c}) = 10°$.

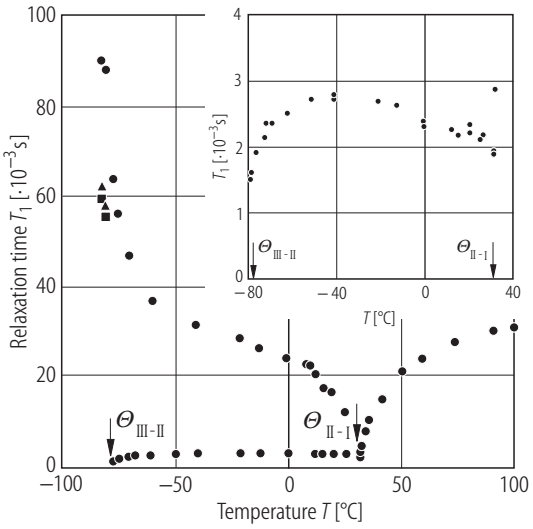

Fig. 39A-10-059. Rb_2ZnCl_4. T_1 vs. T [94Wal]. T_1: spin-lattice relaxation time of the upper frequency ^{87}Rb satellite transition of Rb(1). $\boldsymbol{H} \parallel \boldsymbol{a}$. In phase II, data points indicate T_1 of the edge singularities. Insert: the short T_1 of the edge singularity on an enlarged scale.

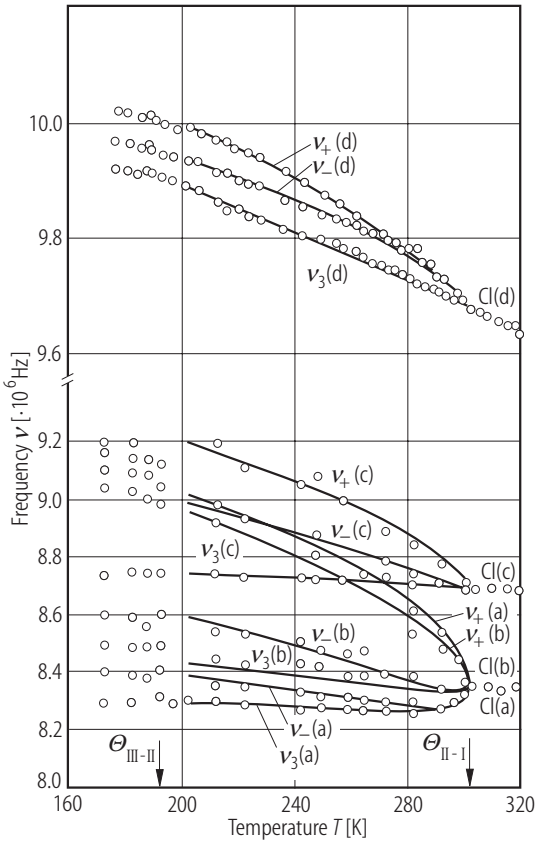

Fig. 39A-10-060. Rb_2ZnCl_4. ν vs. T [81Mil]. ν: ^{35}Cl NQR frequency. Full lines: calculated within the plane-wave model.

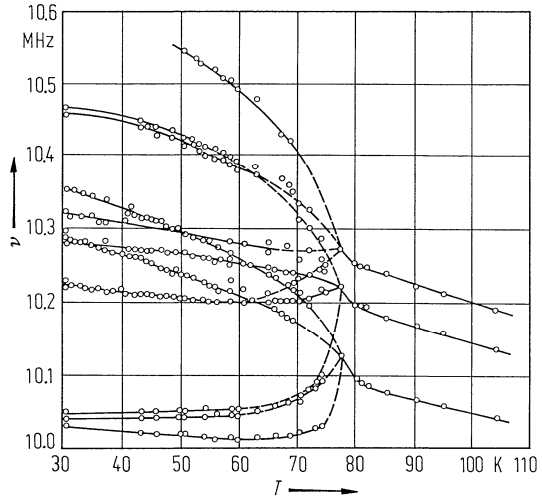

Fig. 39A-10-061. Rb_2ZnCl_4. ν vs. T [83Mur]. ν: ^{35}Cl NQR frequency.

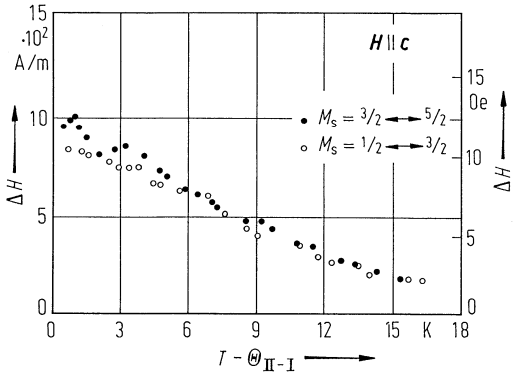

Fig. 39A-10-062. Rb_2ZnCl_4. ΔH vs. $T - \Theta_{II-I}$ [85Kaz]. ΔH: half linewidth for Mn^{2+} ESR spectrum.

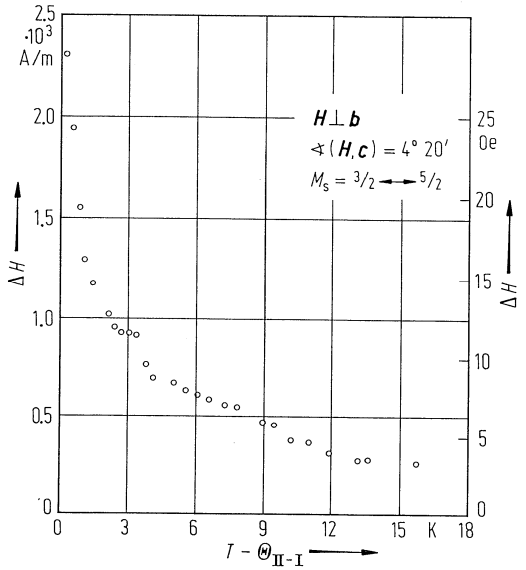

Fig. 39A-10-063. Rb_2ZnCl_4. ΔH vs. $T - \Theta_{II-I}$ [85Kaz]. ΔH: half linewidth for Mn^{2+} ESR spectrum.

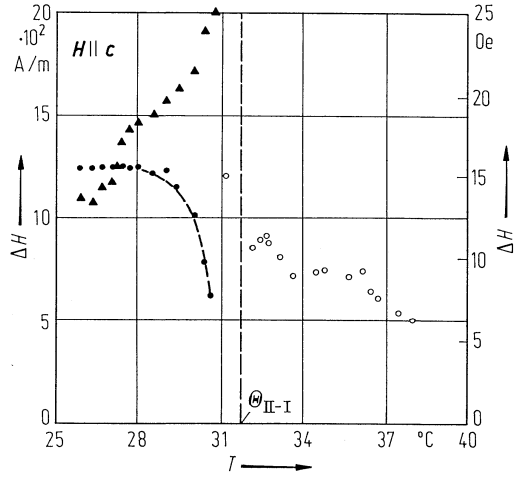

Fig. 39A-10-064. Rb_2ZnCl_4. ΔH vs. T [86Kaz]. ΔH: Mn^{2+} ESR linewidth. Full triangle: low field singularity, full circle: high field singularity, open circle: critical broadening above $\Theta_{II–I}$.

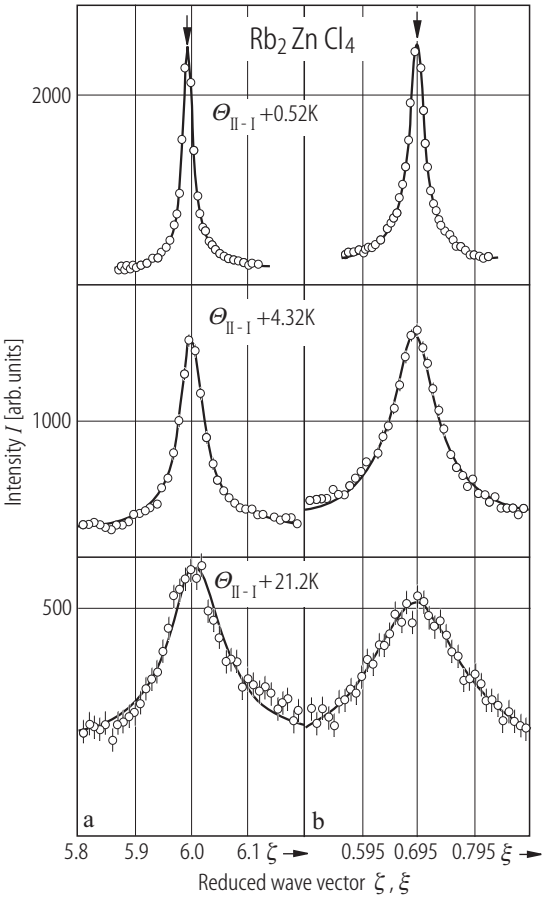

Fig. 39A-10-065. Rb_2ZnCl_4. (**a**) I vs. ζ around (ζ, 0, 2/3 + δ), (**b**) I vs. ξ around (6, 0, ξ) [83And]. I: X-ray scattering intensity. Parameter: T. $\Theta_{II–I}$ = 303.3(1) K. δ: parameter which measures the deviation of the period of the lattice modulation along the c direction from $3c_0$ ($3c_0$: unit cell parameter in phase I).

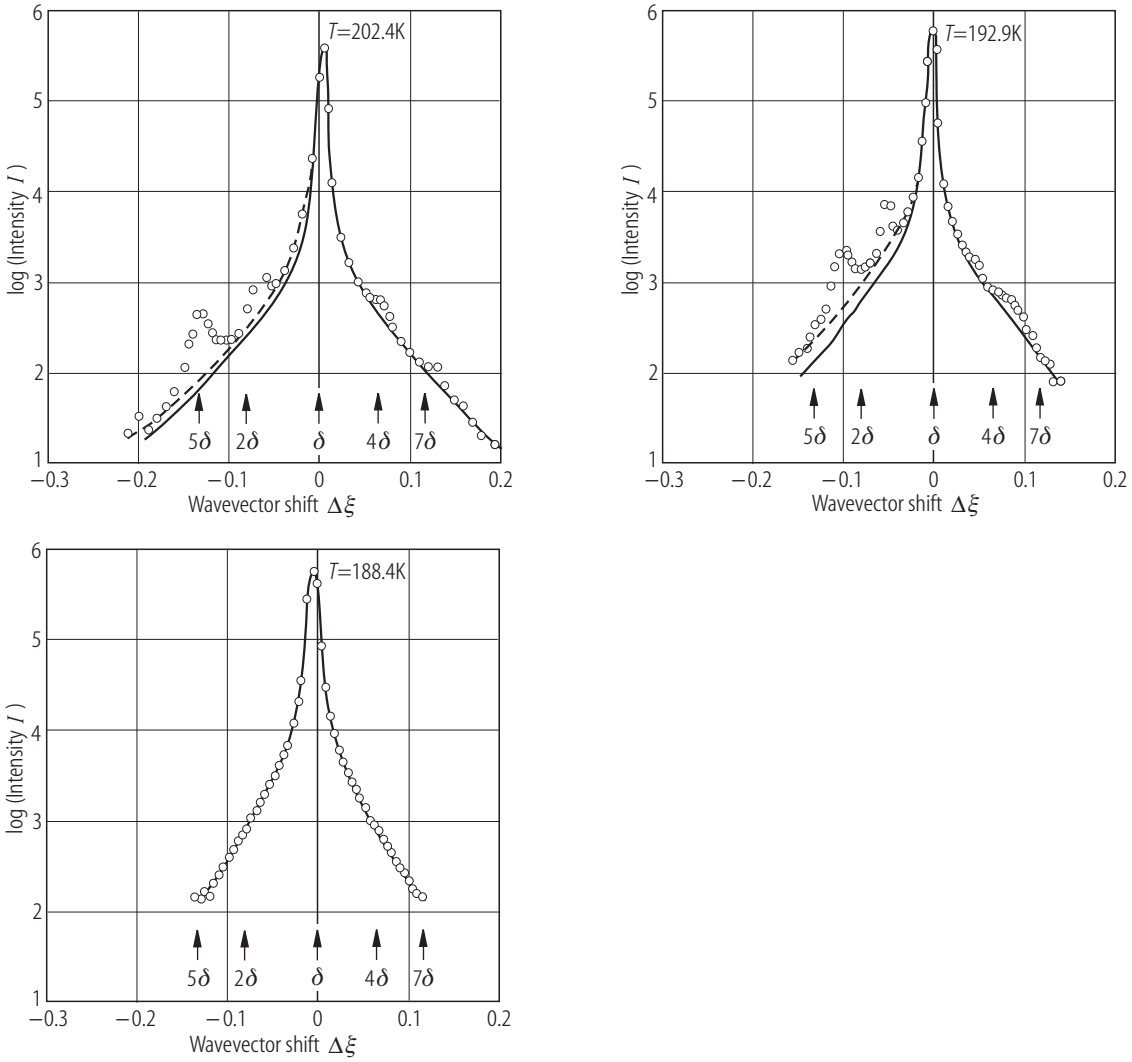

Fig. 39A-10-066. Rb_2ZnCl_4. log$I$ vs. $\Delta\xi$ [83And]. I: X-ray scattering intensity at (6, 0, 2/3 + δ + $\Delta\xi$). Parameter: T. Θ_{III-II} is 186.0(5) K on cooling and 190.0(5) K on heating. Various orders of satellite reflection are indicated by arrows.

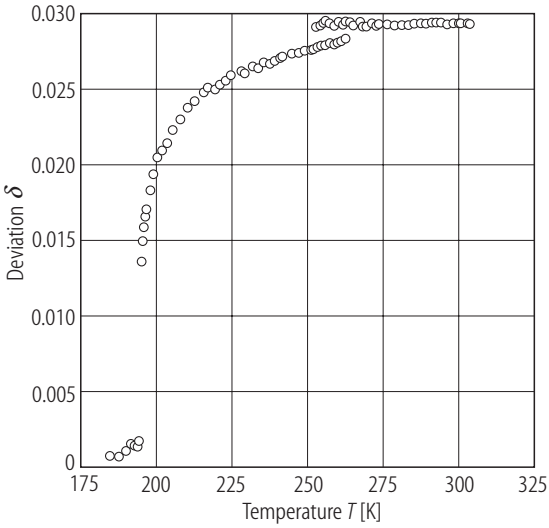

Fig. 39A-10-067. Rb_2ZnCl_4. δ vs. T [87Deg]. For the meaning of δ, see Fig. 39A-10-065. On cooling.

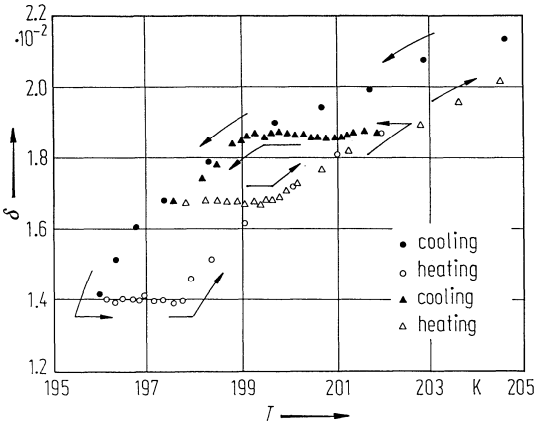

Fig. 39A-10-068. Rb_2ZnCl_4. δ vs. T [87Deg]. For the meaning of δ, see Fig. 39A-10-065. Arrows indicate the direction of temperature variation.

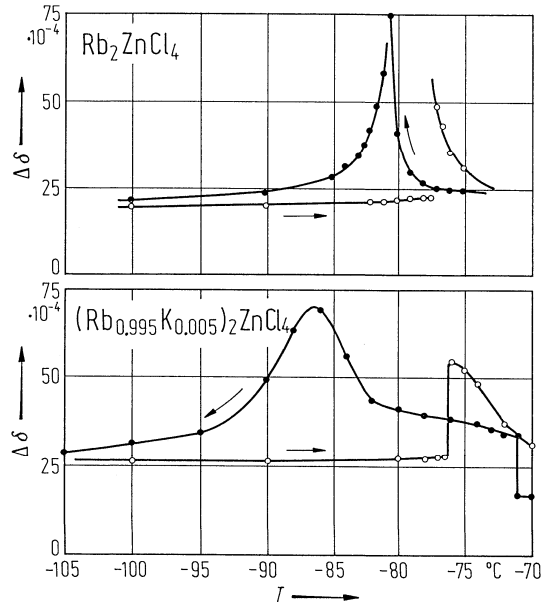

Fig. 39A-10-069. Rb_2ZnCl_4, $(Rb_{0.995}K_{0.005})_2ZnCl_4$. $\Delta\delta$ vs. T [82Mas]. $\Delta\delta$: full width at half maximum of X-ray satellite reflection at (2, 0, 2/3 + δ) scaled by the fraction of c^*. Full circle: on cooling, open circle: on heating.

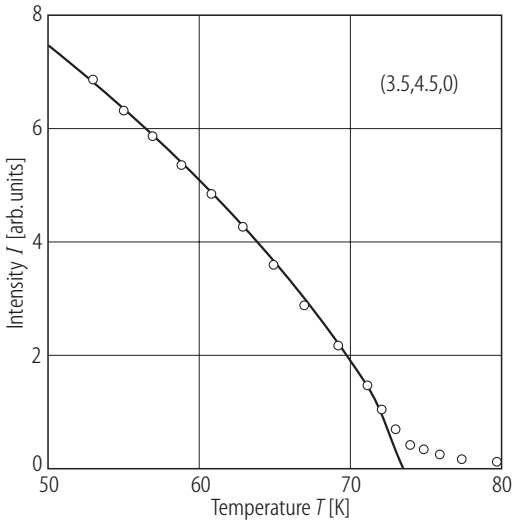

Fig. 39A-10-070. Rb_2ZnCl_4. I vs. T [92Mas]. Neutron scattering. I: integrated intensity of the satellite reflection at (3.5, 4.5, 0). The solid line is a fit to a power law of $I \propto (\Theta_{IV-III} - T)^{2\beta}$ with $\Theta_{IV-III} = 73.5$ K and $2\beta = 0.732$.

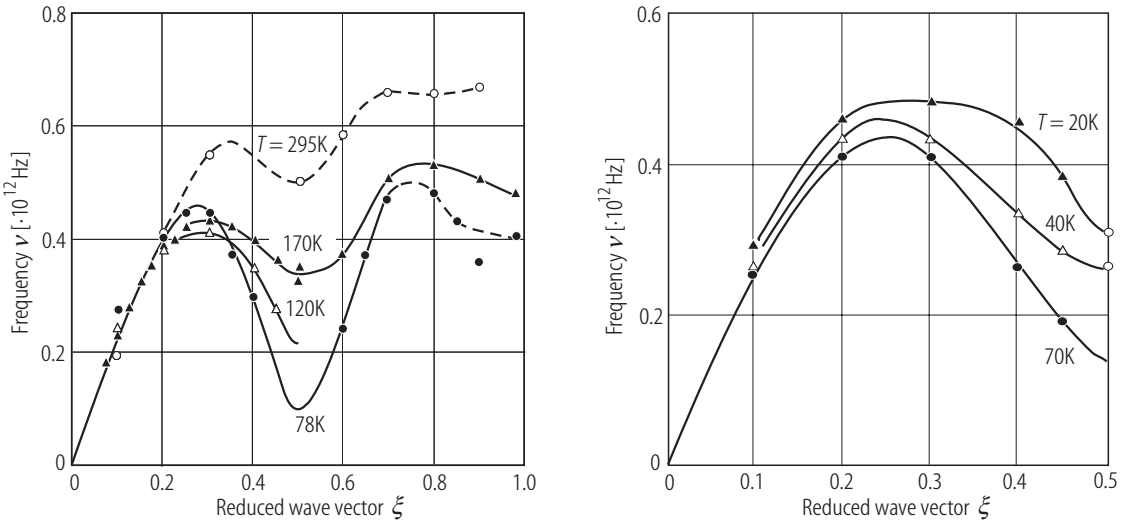

Fig. 39A-10-071. Rb_2ZnCl_4. Dispersion curves for the soft phonon mode along the (ξ, ξ, 0) line [92Mas]. Parameter: T. Neutron scattering. The data points for 295 K are from [91Qui]. Open circles at 20 K and 40 K are Raman frequencies [81Wad].

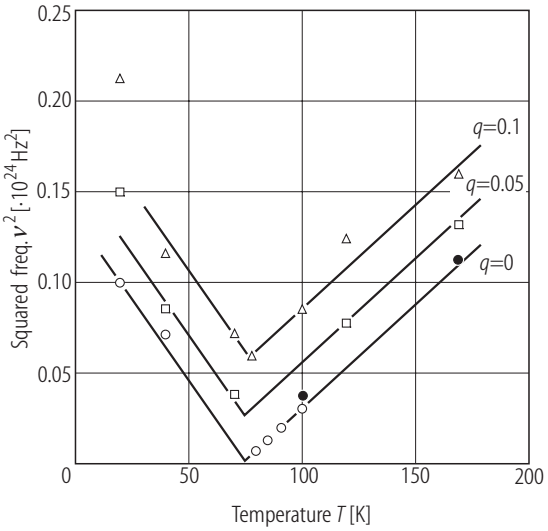

Fig. 39A-10-072. Rb_2ZnCl_4. ν^2 vs. T [92Mas]. ν: frequency of the soft phonons. Scattering vector is $\boldsymbol{Q}$ = (3.5 + q, 4.5 – q, 0). Open circles are data from inelastic neutron scattering (80 K…101 K) [91Qui], and from Raman scattering (20 K, 40 K) [81Wad].

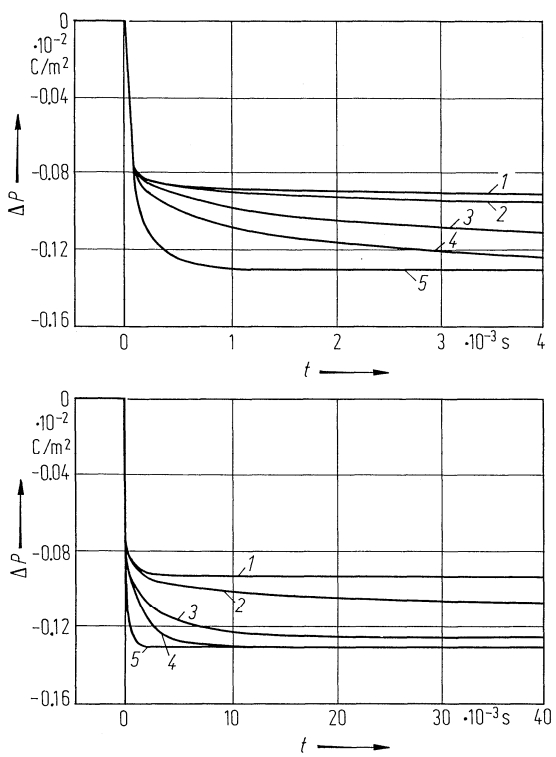

Fig. 39A-10-073. Rb_2ZnCl_4. Time dependence of the change in polarization, ΔP, during the III–II phase transition induced by the removal of dc electric field of $1.8 \cdot 10^6$ V m^{-1} from the specimen [85Ham2]. Upper and lower halves indicate the results during the initial 4 ms and 40 ms, respectively. Curve *1*: $T = T_c^h - 5.08$ K, *2*: $T = T_c^h + 0.05$ K, *3*: $T = T_c^h + 0.45$ K, *4*: $T = T_c^h + 0.63$ K, *5*: $T = T_c^h + 1.58$ K. T_c^h : the transition temperature where the low frequency dielectric constant shows the maximum in heating, 196.17 K.

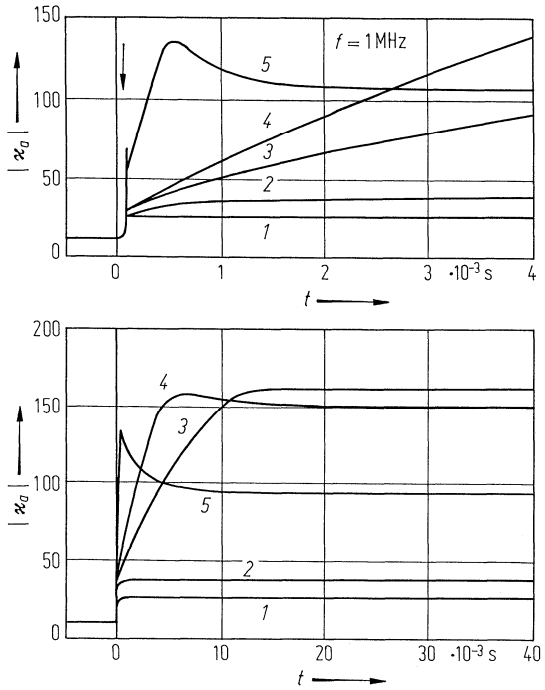

Fig. 39A-10-074. Rb_2ZnCl_4. Time dependence of the absolute value of the complex dielectric constant, $|\varkappa_a|$, during the III–II phase transition induced by the removal of dc electric field of $1.8 \cdot 10^6$ V m^{-1} from the specimen [85Ham2]. Parameter: T. f = 1 MHz. The temperatures for curves *1*...*5* are the same as those in Fig. 39A-10-073.